Int J Earth Sci (Geol Rundsch) (2016) 105:2175–2201
DOI 10.1007/s00531-015-1279-7

ORIGINAL PAPER

Aeromagnetic interpretation in the south-central Zimbabwe Craton: (reappraisal of) crustal structure and tectonic implications

Rubeni T. Ranganai[1] · Kathryn A. Whaler[2] · Cynthia J. Ebinger[3]

Received: 5 June 2015 / Accepted: 28 November 2015 / Published online: 12 December 2015

Abstract Regional aeromagnetic data from the south-central Zimbabwe **C**raton have been digitally processed and enhanced for geological and structural mapping and tectonic interpretation integrated with gravity data, to constrain previous interpretations based on tentative geologic maps and provide new information to link these structural features to known tectonic events. The derived maps show excellent correlation between magnetic anomalies and the known geology, and extend lithological and structural mapping to the shallow/near subsurface. In particular, they reveal the presence of discrete crustal domains and several previously unrecognised dykes, faults, and ultramafic intrusions, as well as extensions to others. Five regional structural directions (ENE, NNE, NNW, NW, and WNW) are identified and associated with trends of geological units and cross-cutting structures. The magnetic lineament patterns cut across the >2.7 Ga greenstone belts, which are shown by gravity data to be restricted to the uppermost 10 km of the crust. Therefore, the greenstone belts were an integral part of the lithosphere before much of the upper crustal (brittle) deformation occurred. Significantly, the observed magnetic trends have representatives craton-wide, implying that our interpretation and inferences can be applied to the rest of the craton with confidence. Geological–tectonic correlation suggests that the interpreted regional trends are mainly 2.5 Ga (Great Dyke age) and younger, and relate to tectonic events including the reactivation of the Limpopo Belt at 2.0 Ga and the major regional igneous/dyking events at 1.8–2.0 Ga (Mashonaland), 1.1 Ga (Umkondo), and 180 Ma (Karoo). Thus, their origin is here inferred to be inter- and intra-cratonic collisions and block movements involving the Zimbabwe and Kaapvaal Cratons and the Limpopo Belt, and later lithospheric heating and extension associated with the break-up of Gondwana. The movements produced structures, or reactivated older fractures, that were exploited by Late Archaean and Proterozoic mafic intrusions. There was interplay between vertical and horizontal tectonics as seen in similar terrains worldwide.

Keywords Zimbabwe **C**raton · Limpopo Belt · Aeromagnetic anomalies · Structural trends · Crustal domains · Tectonic evolution

Abbreviations

AFTT	Apatite fission-track thermochronology
BIF	Banded iron formation
BKD	Botswana Karoo dyke (swarm)
BGS	Botswana geological survey
CGS	Council for geosciences (South Africa)
CZ	Central zone (Limpopo Belt)
ED	East dyke
FRD	Fort Rixon dykes
GD	The Great Dyke
KC	Kaapvaal craton
LB	Limpopo belt
MCD	Mashava-Chivi dykes
NLTZ	North limpopo thrust zone
NMZ	North marginal zone (Limpopo Belt)

✉ Rubeni T. Ranganai
ranganai@mopipi.ub.bw

[1] Physics Department, University of Botswana, P. Bag UB0704, Gaborone, Botswana

[2] School of GeoSciences, University of Edinburgh, Grant Institute, James Hutton Road, Edinburgh EH9 3FE, UK

[3] Department of Earth and Environmental Sciences, 227 Hutchison Hall, University of Rochester, Rochester, NY 14627, USA

SMZ South marginal zone (Limpopo Belt)
SPD Sebanga Poort dyke
UD Umvimeela dyke
ZC Zimbabwe **C**raton
ZGS Zimbabwe geological survey

Introduction

Discussions of the tectonic development of the Archaean Zimbabwe **C**raton rely significantly on the geological interpretation of the field relations and patterns of the granites, greenstones, and mafic dykes of the south-central part of the country, including part of the Neoarchaean Limpopo Belt (LB) (Figs. 1, 2; Wilson et al. 1987; Wilson 1990; Campbell et al. 1992; Bickle and Nisbet 1993; Fedo et al. 1995; Wilson et al. 1995). Most parts of this region are reasonably exposed and now geologically well mapped and sampled (e.g. Bickle and Nisbet 1993; Fedo et al. 1995; Frei et al. 1999; Horstwood et al. 1999; Jelsma et al. 1996, 2004; Prendergast 2004; Prendergast and Wingate 2007). Over the last two decades, geochronological, palaeomagnetic, and geochemical data have also contributed to the geotectonic interpretation of the region and the craton as a whole (Mushayandebvu et al. 1995; Wilson et al. 1995; Horstwood et al. 1999; Jelsma and Dirks 2002; Jelsma et al. 2004; Söderlund et al. 2010). However, most of the existing interpretations are generally hampered by the lack of regional structural and/or kinematic data and constraints on the subsurface

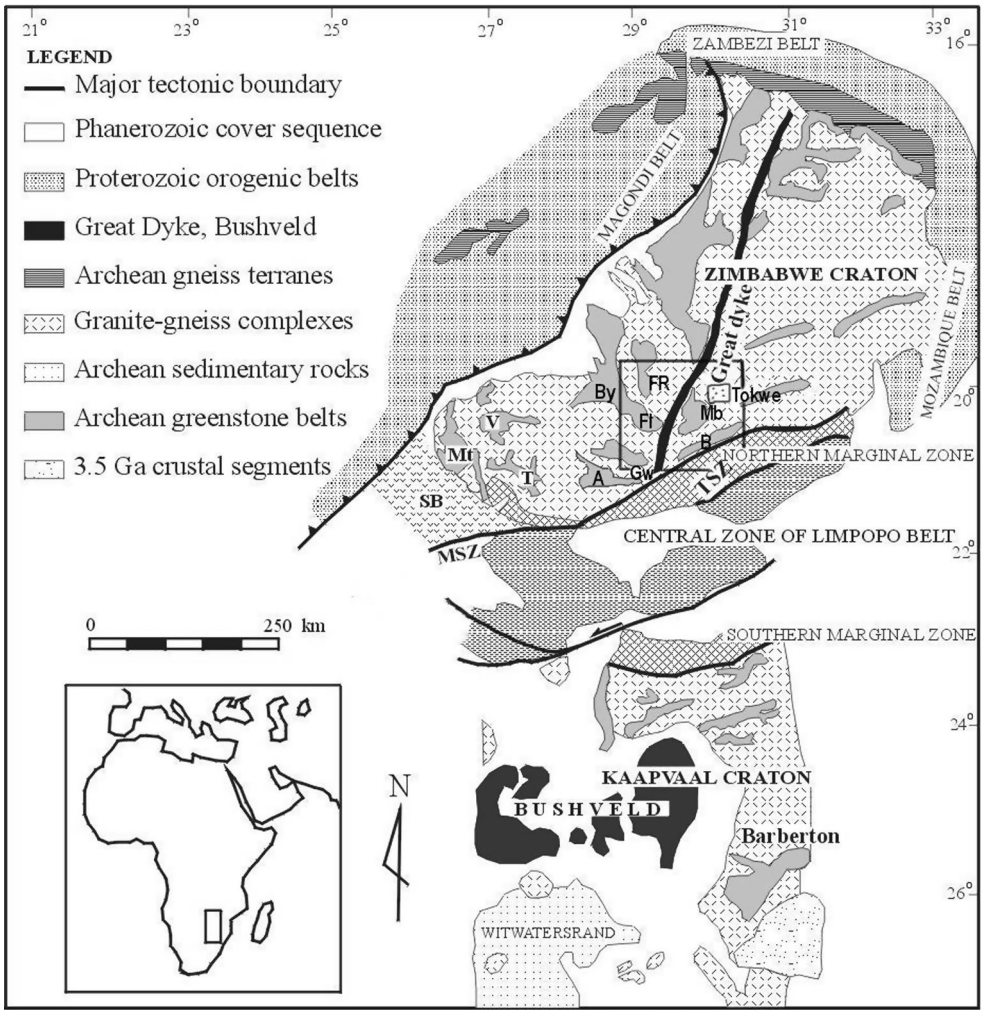

Fig. 1 Map showing the main geological units of the southern Africa (Azanian) Craton and adjacent Proterozoic Belts (After Ranganai et al. 2002; Kampunzu et al. 2003). The main features of the *Zimbabwe* ***C****raton and the Limpopo Belt* as mentioned in the text are illustrated. Greenstone belts: *A* Antelope, *B* Buhwa, *By* Bulawayo, *Fl* Filabusi, *FR* Fort Rixon, *Gw* Gwanda, and *Mb* Mberengwa; *Mt* Matsitama, *V* Vumba, *T* Tati; *MSZ* and *TSZ* identify the *Magogaphate and Triangle shear zones*, respectively. *SB* Shashe Belt that forms the Limpopo–Shashe Belt of Ranganai et al. (2002). The *rectangle* locates the study area (Fig. 2). *Index map* shows the location of the Azanian Craton in Africa

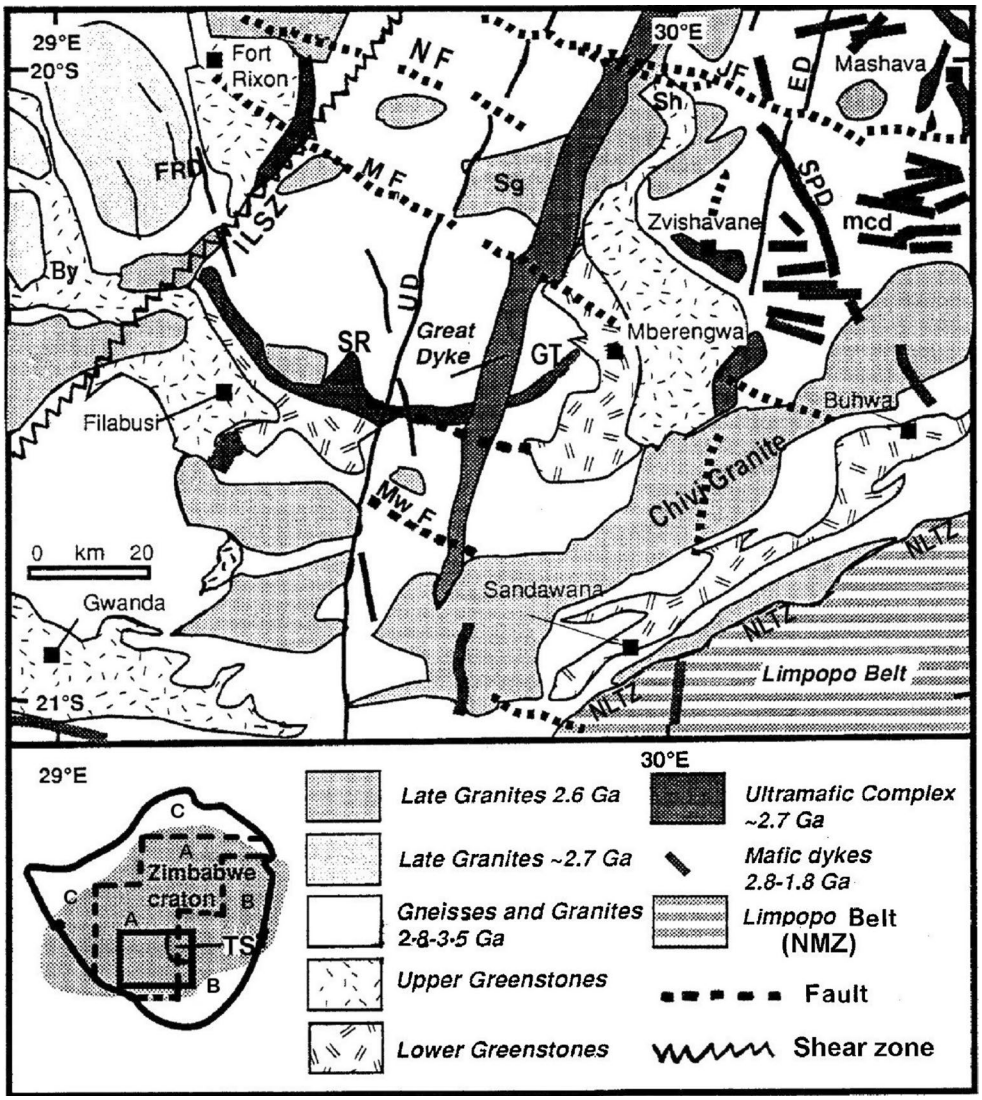

Fig. 2 Simplified geological map of the study area, south-central Zimbabwe **C**raton. *TS* (see insert) ~3.5 Ga Tokwe Segment (*north-eastern area* between Zvishavane and Mashava), *ED* East dyke, *mcd* Mashava-Chivi dykes, *FRD* Fort Rixon dykes, *GT* Gurumba Tumba ultramafic; *SPD* Sebanga Poort dyke, *SR* Shamba Range ultramafic, *UD* Umvimeela dyke, *ILSZ* Irisvale–Lancaster Shear Zone, *JF* Jenya fault, *MF* Mchingwe fault, *Mw F* Mwenezi fault, *NF* Ngomi fault, *Sg* Shabani granite, *Sh* Snake head section (Mberengwa greenstone belt). Greenstone belts are named after respective towns. *Index map* shows study area (*continuous box*) and the Tokwe segment (*TS*) within the Zimbabwe Craton, and the aeromagnetic survey blocks (A-1983; B-1988; C-1990)

geometry of structures, information that is obtainable from geophysical data analyses.

Gravity and magnetic data are particularly crucial in revealing density and magnetisation or susceptibility contrasts that depend upon rock type (lithology), alteration, structure and subsurface geometry, and disposition (e.g. Clark 1997; Jaques et al. 1997; Gibson and Millegan 1998; Airo 2002; Bauer et al. 2003; Betts et al. 2003; Nabighian et al. 2005; Allek and Hamoudi 2008). In particular, magnetic data can provide a link between outcropping rock and the subsurface, and help to solve problems of crustal architecture, overprinting relationships, and kinematics (e.g. Betts et al. 2003, 2007; Aitken et al. 2008; Aitken and Betts 2009; Stewart et al. 2009). In this regard, Ranganai and Ebinger (2008) used available regional aeromagnetic data from the region for structural mapping applied to hydrogeologic purposes, while Ranganai (2012) has used Euler deconvolution and spectral analysis in an attempt to obtain some regional depth constraints on these structures. The current study expands on these studies and integrates gravity interpretation (e.g. Ranganai et al. 2008) in an attempt to unravel the geotectonic evolution of the region. The aeromagnetic data are used to generate a more complete picture of the tectonic evolution of the south-central Zimbabwe **C**raton through the combination of current and previous interpretations and a more regional perspective.

The objectives of this study were (1) to correlate the known geology with magnetic anomalies and their derivatives, and extend mapping to depth (shallow/near subsurface) and to areas of poor rock exposure, (2) to map regional structural features and discuss their geodynamical implications for the tectonic evolution of the area using their geometry and cross-cutting relations, and (3) to examine the Zimbabwe **C**raton–Limpopo Belt (ZC-LB) contact relationship and consider the cause-and-effect link between

Table 1 Major stratigraphic subdivision and chronology of the Zimbabwe Craton and the Mberengwa Greenstone Belt (After Wilson 1990; Taylor et al. 1991; Bickle and Nisbet 1993; Wilson et al. 1995; Jelsma et al. 1996, 2004; Horstwood et al. 1999; Stubbs 2000)

Age (Ga)	Zimbabwe **C**raton (e.g. Taylor et al. 1991)	Study area (e.g. Bickle and Nisbet 1993)	Lithology
2.57 (2.6)	Chilimanzi suite (granitoids)	Chilimanzi suite (granitoids)	K-rich
2.67	Sesombi/wedza Suite (granitoids)	Sesombi suite (granitoids)	Na-rich
2.70	Shamvaian group	Not preserved	Clastic? sediments
	Bulawayan group	Belingwean group	
2.70	Upper greenstones	Ngezi group	Komatiitic/tholeiitic basalts
2.90	Lower Greenstones	Mtshingwe group	Ultramafic rocks?
2.8–2.9	Tonalites	Tonalites	
3.0		Buhwa greenstone belt (Fedo et al. 1995)	Shelf-sediments
3.50	Sebakwian group	Tokwe segment schist inclusions (e.g. Horstwood et al. 1999)	Mafic/ultramafic rocks
3.80		Zircons from greenstone belts	

the two terranes. The results of the aeromagnetic interpretation are integrated with previous palaeomagnetic and gravity studies and geological models to elucidate the tectonic evolution of the region, and relate this to the evolution of the Zimbabwe **C**raton as a whole. It is the joint consideration of the many 'products' derived from the anomaly data with other geoscience data that gives the final interpretation its strength.

Regional geology and tectonics

The study area is located in the south-central part of the Archaean Zimbabwe **C**raton and includes a small portion of the ENE-trending adjacent Limpopo Orogenic Belt which extends into South Africa and Botswana (Figs. 1, 2). Three major phases of greenstone development are recognised in the craton, namely the ~3.5 Ga Sebakwian Group, ~2.9 Ga Lower Greenstones, and 2.7 Ga Upper Greenstones (Table 1, e.g. Taylor et al. 1991; Wilson et al. 1995; Jelsma et al. 1996; Blenkinsop et al. 1997; Horstwood et al. 1999; Jelsma and Dirks 2002; Prendergast 2004). The Limpopo Belt consists of reworked granitoid–greenstone rocks of the craton and a magmatic plutonic assemblage at amphibolite and/or granulite facies metamorphism (Roering et al. 1992; Rollinson and Blenkinsop 1995; Holzer et al. 1999), in thrust contact with cratonic granitoids (Mkweli et al. 1995; Frei et al. 1999). The granulite rocks contain several inclusions of greenstone belt remnants, metabasites, mafic dykes, ultramafics, and magnetite quartzites/banded iron formation, as narrow layers several kilometres long (Rollinson and Blenkinsop 1995). On the basis of structure and metamorphic grade (e.g. Roering et al. 1992), this belt can be divided into a north marginal zone (NMZ) wholly within Zimbabwe; a central zone (CZ) partly in Zimbabwe, Botswana, and South Africa; and a south marginal zone (SMZ) in South Africa (Fig. 1). The Zimbabwe **C**raton–Limpopo Belt (ZC-LB) boundary is traditionally taken as the orthopyroxene isograd (Coward et al. 1976), but a structural break, the North Limpopo Thrust Zone (NLTZ; Fig. 2), is now recognised (e.g. Blenkinsop 2011; Blenkinsop et al. 1995; Mkweli et al. 1995; Rollinson and Blenkinsop 1995; Ranganai 2012), with the LB thrust over the ZC. Ranganai et al. (2002) have used a compilation of regional gravity data to redefine the extent of the Limpopo Belt to include the Shashe Belt in Botswana which forms a southward convex orogenic arc between the Kaapvaal and Zimbabwe **C**ratons (Fig. 1).

The oldest part of the study area is the ~3.5 Ga Tokwe Segment (TS, index map in Fig. 2) comprising highly deformed and banded tonalitic (TTG) gneisses, whose ~NS trend also defines the >3.1 Ga tectonic grain of the craton (Wilson 1990; Campbell et al. 1992; Wilson et al. 1995; Horstwood et al. 1999; Dodson et al. 2001). This unique terrain is considered to be a nucleus, from where the craton grew westwards and northwards by crustal accretion (Wilson 1990; Wilson et al. 1995; Dirks and Jelsma 1998, 2002; Kusky 1998; Horstwood et al. 1999; Jelsma and Dirks 2002). However, recent geochronological work north-west of the segment suggests that this 'proto-craton' is not as extensive as previously argued by some authors (Jelsma et al. 2004). The Tokwe Segment contains remnants of the Early Archaean greenstone rocks (Wilson 1990), forms the basement to younger greenstones (Bickle and Nisbet 1993; Blenkinsop et al. 1997; Fedo et al. 1995; Hunter et al. 1998), and is extensively intruded by younger granites and mafic dyke swarms (e.g. mcd, Fig. 2; Wilson et al. 1987; Bickle and Nisbet 1993; Prendergast 2004). In particular, an extensive suite of tonalite–trondjhemite–granitoid (TTG) associated with the Lower Greenstones intruded the segment at

2.9–2.8 Ga (Chingezi suite), and represents one of the main crust-forming events in the craton (Taylor et al. 1991; Wilson et al. 1995; Jelsma et al. 1996, 2004; Horstwood et al. 1999). Recent work recognises an equally important tectono-magmatic event at 2.7 Ga that produced the two distinct greenstone successions (Jelsma and Dirks 2002).

The greenstone belts of the area (Fig. 2) are generally characterised by sequences of ultramafic, mafic, and felsic volcanic and volcano–sedimentary assemblages mainly at greenschist facies metamorphism but rising to amphibolite facies at their margins (Bickle and Nisbet 1993; Wilson et al. 1995; Blenkinsop et al. 1997). The general regional stratigraphy includes the ~2.9 Ga Lower Greenstones (the Belingwean), the widespread and dominant 2.7 Ga Upper Greenstones, and minor 2.7–2.65 Ga Shamvaian-type sediments (Fig. 2; Table 1; e.g. Bickle and Nisbet 1993; Wilson et al. 1995; Jelsma and Dirks 2002). The greenstone belts are commonly believed to be emplaced in pre-existing continental crust with magma derived from a mantle plume (e.g. Bickle et al. 1994; Blenkinsop et al. 1997; Wilson et al. 1995; Hunter et al. 1998; Bolhar et al. 2003; Kamber et al. 2004; Prendergast 2004; Prendergast and Wingate 2007; Ranganai et al. 2008). Subsequent compressional deformation is then attributed to vertical processes, including liquid and solid-state granite diapirism or ballooning plutonism followed by late-stage strike-slip activity (Jelsma et al. 1993; Blenkinsop et al. 1997; Becker et al. 2000; Siegesmund et al. 2002; Ranganai et al. 2008; Ranganai 2013). It is also possible that the dominant regional pattern now seen may have been acquired in part prior to the main phase of Late Archaean deformation and granitoid emplacement which then modified, rather than produced, the basic geometry of the greenstone belts (Campbell et al. 1992). Other workers argue that the greenstone belts represent fragments of oceanic crust, oceanic plateaus, or island arcs laterally amalgamated with continental fragments during some form of subduction–accretion (Dirks and Jelsma 1998, 2002; Kusky 1998; Jelsma and Dirks 2000, 2002; Dirks et al. 2002; Hofmann et al. 2003; Hofmann and Kusky 2004). The main exception in terms of stratigraphy is the ~3.0 Ga Buhwa greenstone belt of sedimentary and subordinate volcanic rocks, which do not correlate with the Lower Greenstones with which they have been previously associated (Table 1; Fedo et al. 1995). Rollinson (1993) also suggests an allochthonous origin for the greenstone belt, as well as the Matsitama greenstone belt on the south-western edge of the craton in north-east Botswana (Mt, Fig. 1), while Fedo and Errikson (1996) have interpreted it as a stable-shelf succession. Detailed discussions and revisions of the greenstone stratigraphy and craton evolution can be found in Wilson et al. (1995), Blenkinsop et al. (1997), Horstwood et al. (1999), Jelsma and Dirks (2002), Bolhar et al. (2003).

Several layered ultramafic intrusions and mafic dykes of various ages are scattered throughout the area. The ultramafic intrusions have previously been considered to be Pre-Upper Greenstones and to be related to the Lower Greenstone volcanism, representing a period of increased mantle activity with intrusion and brittle fracturing in the crust (Wilson 1990). However, recent zircon geochronology from one of these ultramafic complexes, the Mashaba Igneous Complex (Ma, Fig. 2), gives a precise age of 2.75 Ga, about 50 Ma older than previously estimated (Prendergast and Wingate 2007), thus linking them to the sub-volcanic phases of komatiitic sill-flow complexes (i.e. same magmatic event as the Upper Greenstones). Three sets of dyke swarms of Archaean age (~2.7 Ga; Stubbs 2000) forming a modified radial and ring pattern possibly related to a major volcanic centre, the Mashava-Chivi dykes (Wilson et al. 1987; MCD, Fig. 2), are restricted to the ~3.5 Ga Tokwe Segment (Fig. 2; Wilson 1990; Wilson et al. 1995), and appear to be intimately related to the tectonic processes that produced the main Archaean granite–greenstone terrains. They are considered, together with the associated Mashava Igneous Complex (Ma), to be part of the feeder system to basaltic lavas of the 2.7 Ga Upper Greenstones which dominate the greenstone succession (Wilson 1990; Wilson et al. 1987, 1995; Stubbs 2000; Prendergast 2004). They cut the basement gneisses but are absent from the ~2.6 Ga Chilimanzi granites and in places are seen to be cut by these granites (Wilson et al. 1987). A few Proterozoic dykes of the Mashonaland Igneous Event (~1.8–2.0 Ga) are mapped east and west of the Mberengwa (Belingwe) and Fort Rixon greenstone belts, respectively (e.g. SPD, FRD, Fig. 2). The dykes are considered to be feeders to the ubiquitous Mashonaland dolerite sills of north-eastern and eastern Zimbabwe (Wilson et al. 1987; Wilson 1990; Mushayandebvu et al. 1995; Hanson et al. 1998, 2006). However, according to Söderlund et al. (2010), three samples of WNW- to NNW-trending dykes of the Sebanga swarm yielded ages of 2512.3 ± 1.8, 2470.0 ± 1.2, and 2408.3 ± 2.0 Ma, the last of which dates the Sebanga Poort dyke of this swarm thus invalidating a genetic link between the SPD and the Mashonaland sills.

'Young' granite plutons, 2.7–2.65 Ga Sesombi and Wedza and 2.6 Ga Chilimanzi suites, intrude and deform both the older gneisses and the greenstone belts (Wilson et al. 1995; Jelsma et al. 1996; Horstwood et al. 1999). These are in turn cut by the ~2.57 Ga NNE-striking mafic–ultramafic Great Dyke and its nearly parallel mafic (gabbroic) satellite dykes and features (e.g. Umvimeela and East dykes, UD and ED, Fig. 2), which have been termed the Great Dyke fracture system (Wilson 1990; Wilson et al. 1987, 1995). Their formation has been linked with the collision between the Zimbabwe and Kaapvaal Cratons (Wilson 1990), and the creation of the Limpopo orogenic belt

(Oberthür et al. 2002; Schoenberg et al. 2003). This fracture system and the dyke emplacement are seen as indicating the onset of a phase of significant crustal extension in the craton (Campbell et al. 1992). Mukasa et al. (1998) argue that emplacement of the Great Dyke and its satellite dykes was contemporaneous with emplacement of the youngest of the TTG suite at about 2596 Ma. However, this is highly unlikely since the dyke cuts granites and the craton must have behaved brittlely to accommodate the satellite dykes and accompanying fractures (Oberthür et al. 2002; Schoenberg et al. 2003; H. Jelsma pers. com. 2007).

Several workers seek an interrelationship of events in the craton and the adjacent orogenic belt to explain their mutual tectonic development (e.g. Wilson 1990; Treloar et al. 1992; Fedo et al. 1995; Frei et al. 1999; Nguuri et al. 2001; Oberthür et al. 2002; Kampunzu et al. 2003; Gore et al. 2009; Khoza et al. 2013). A variety of models have been formulated about the tectonic evolution and structure of the Limpopo Belt, and a review of the various models of its formation can be found in several articles (Blenkinsop 2011; Gwavava et al. 1992; Roering et al. 1992; Rollinson 1993; Kamber et al. 1995; Holzer et al. 1999; Khoza et al. 2013). On the basis of geochronological data, it has been argued that the Limpopo Orogeny occurred during the Neoarchaean (2.7–2.6 Ga), with a major reactivation event during the Paleoproterozoic at 2.0 Ga (e.g. Treloar et al. 1992; Barton et al. 1994; Kamber et al. 1995; Holzer et al. 1999; Schaller et al. 1999; Bumby et al. 2004). Rocks in the two marginal zones reportedly underwent a single granulite facies metamorphism in the Neoarchaean (Kreissig et al. 2001; Blenkinsop et al. 2004; Bumby et al. 2004), while the CZ was affected by two distinct high-grade events, one in the Neoarchaean and the other in the Palaeoproterozoic (Kamber et al. 1996; Bumby et al. 2004; Boshoff et al. 2006). Geological, structural, and geophysical data appear to favour an interpretation of the crustal structure as intercratonic uplift related to continent–continent collision, with the CZ interpreted as a Neoarchaean collisional pop-up structure (or flower structure?) (de Wit et al. 1992; Mkweli et al. 1995; De Beer and Stettler 1992; Ranganai et al. 2002). Gravity, electromagnetic, and seismic studies support structural evidence that the granulitic SMZ and NMZ were thrust onto the adjacent cratons at shallow angles (De Beer and Stettler 1992; Durrheim et al. 1992; Gwavava et al. 1992; Mkweli et al. 1995; Holzer et al. 1999).

On the basis of the above, the geostructural framework of the area can be summarised as follows. Crustal shortening related to the Limpopo Orogeny (e.g. Coward et al. 1976; Roering et al. 1992; Holzer et al. 1999) was followed by wrench and strike-slip deformation that produced the Mchingwe and Jenya dextral faults (Fig. 2, e.g. Stowe 1980; Wilson 1990; Campbell et al. 1992). A reconstruction of igneous–tectonic events in the area based on remote sensing, field studies, and past mapping (Stowe 1980; Wilson 1990; Carruthers et al. 1993; Campbell and Pitfield 1994; Blenkinsop and Treloar 1995; Ranganai and Ebinger 2008) indicates that the geological development of the craton was punctuated by repeated episodes of compressive tectonism involving at least four periods of important wrench faulting separated by relaxation and dyke emplacement. Faults and shear zones with protracted histories of reactivation are common (Campbell et al. 1992; Dirks and Jelsma 2002). Wilson (1990) considers horizontal tectonics involving inter- and intra-cratonic block movements to be the important factor (see also Treloar and Blenkinsop 1995; Blenkinsop 2011). However, limited gravity studies (Ranganai 1995, 2013; Ranganai et al. 2008; Gwavava and Ranganai 2009) suggest that granite–greenstone relationships are strongly influenced by post-volcanic gravity-induced vertical tectonics (e.g. Jelsma et al. 1993; Blenkinsop et al. 1997; Becker et al. 2000), within regionally compressive stress fields (Jelsma and Dirks 2000). Dirks and Jelsma (1998, 2002) argue that lateral accretion of hot crustal segments must have occurred to provide the thermal driving mechanism for the large-scale diapiric events that resulted in final cooling and stabilisation of the craton. Some workers have related deformation of the granite–greenstone terrane in the area to far-field stresses associated with collisional processes at plate margins (e.g. indenter tectonics related to the Limpopo Belt: Coward et al. 1976; Wilson 1990; Treloar et al. 1992; Treloar and Blenkinsop 1995). It is therefore clear that the relative importance of horizontal, as opposed to vertical, tectonics is still controversial. Resolution of this controversy is important for a full understanding of crustal growth processes in the Zimbabwe **C**raton, and the diversity of Archaean tectonics (Prendergast 2004). We report on the contribution that processed and enhanced magnetic data can make to crustal studies and evaluation and/or discrimination of geotectonic models (cf. Aitken and Betts 2009).

Aeromagnetic data and processing

The aeromagnetic data used in this study were obtained from the Zimbabwe Geological Survey (ZGS) and are based on two regional surveys in 1983 and 1988 covering most of the craton (A and B, Fig. 2). The magnetic data were collected along 1-km-spaced flight lines at 305 m constant mean terrain clearance using Geometrics proton precession and Scintrex caesium vapour magnetometers with resolutions of 0.1 nT and 0.001 nT, respectively. Flight directions were E–W (A, 1983 survey) and N–S (B, 1988 survey), approximately perpendicular to the dominant geological trends in each area, that of greenstone belts (Fig. 2). Tie-lines were flown 14 km apart and the

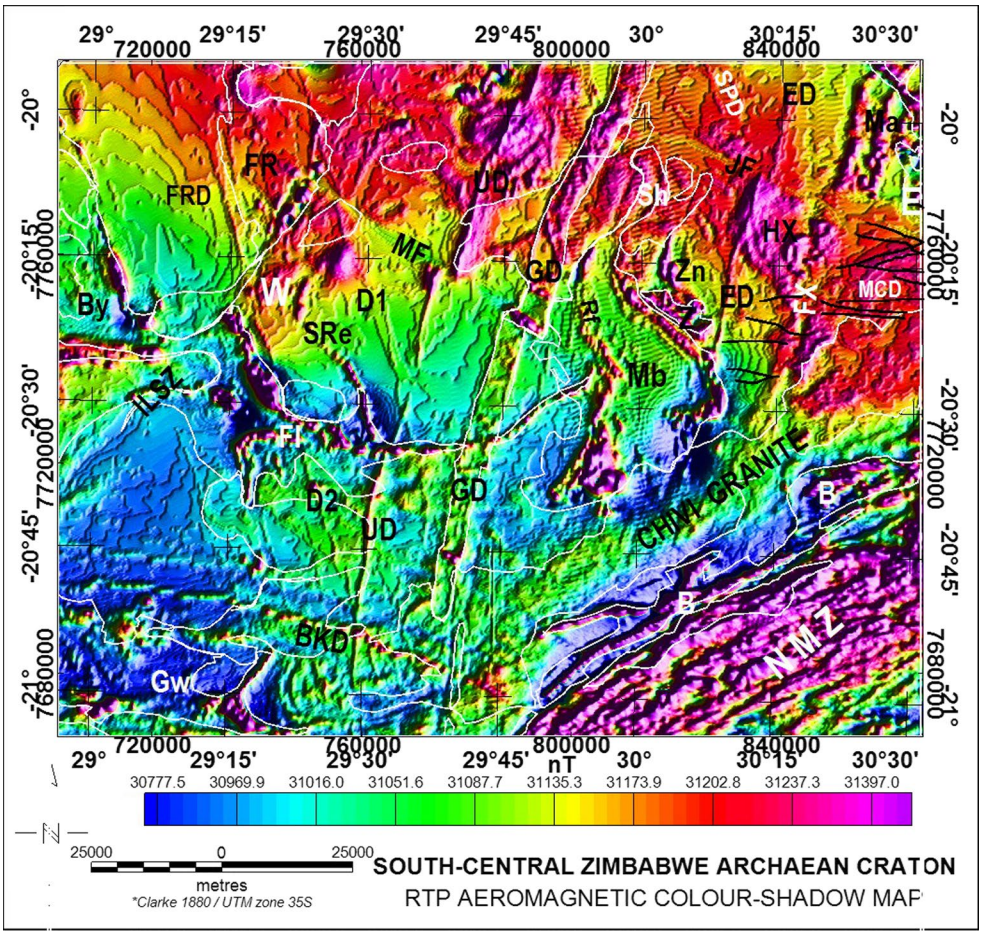

Fig. 3 RTP aeromagnetic *colour-shadow* map (HSV) with known outlines of geological units in *white* (see Fig. 2). Greenstone belt labels/symbols as in Figs. 1, 2; other units: *Ma* Mashava ultramafic complex, *MCD* Mashava-Chivi dykes, *SRe* Shamba Range extension, *Z* Zvishavane ultramafic complex, *Zn* Zvishavane ultramafic extension. *BKD*, *D1*, *D2*, *HX*, *FX* are magnetic anomalies discussed in text. Note magnetic high over Reliance formation (*Rf*) which acts as a stratigraphic (magnetite-rich?) *marker horizon around* the Mberengwa (*Mb*) greenstone belt

data levelled using a combined computer–manual method. Data from the two surveys were combined following the procedure discussed by Barritt (1993). The levelled flight line data were first gridded in the UTM coordinate system at 250-m cell size, i.e. equal to ¼ of the line spacing (see Nabighian et al. 2005), using a bidirectional algorithm (Smith and Wessel 1990). They were then reduced to the pole (RTP, Fig. 3) to correct for the effect of the magnetic inclination (average of −60° in the study area), using algorithms that cater for both high- and low-magnetic latitudes (Geosoft 2004). For purely induced magnetisation, or minimal remanent magnetisation, RTP allows the typically complex observed magnetic anomalies to be shifted in phase to produce the simpler shapes that are expected to lie directly over the magnetic sources (Blakely 1995; Nabighian et al. 2005), thus producing anomaly maps that can be more readily correlated to the near-surface geology, our targets.

The RTP grid was analysed further by frequency domain digital filter operators and enhancement techniques, particularly those designed to enhance shallow, short-wavelength features for lithological contact and structural mapping. These include apparent susceptibility mapping, shaded relief imaging, colour-shadow maps, and vertical and horizontal derivatives (e.g. Broome 1990; Lee et al. 1990; Blakely 1995; Jaques et al. 1997; Reeves et al. 1997; Pilkington and Keating 2004; Verduzco et al. 2004; Cooper and Cowan 2007). However, for the purpose of regional crustal structure, intermediate- or medium-to-long-wavelength anomalies are useful (e.g. Gibson and Millegan 1998). In this case, pseudo-depth slicing (depth ensemble filtering) and an upward continuation filter (e.g. Blakely 1995; Talwani et al. 2003; Nabighian et al. 2005) were used to attenuate the high-frequency anomalies, leaving responses from larger-scale and/or deeper features. Pseudo-depth slicing is a filtering technique used to isolate anomalies based on wavelength criteria by calculating the contribution of selected depth intervals to the total magnetic field (Spector and Grant 1970). These depth intervals are related to slope segments in the energy spectrum for any given data set. Interpretation of different depth-slice images can be used to determine the thickness of different magnetic bodies and establish their progressive changes with depth (Talwani et al. 2003). Available regional gravity data are used

Table 2 A comparison of the computed apparent susceptibility values and measured susceptibilities for the main rock types of the study area, including NRM intensities

Rock unit/type	*N* samples	χ range ($\times 10^{-3}$ SI)	Apparent susceptibility values ($\times 10^{-3}$ SI)	Average (Ns = 3) NRM (mA/m)
Gneisses	8	0.00–0.40	–	–
Granites	27	0.00–0.32	0.00–0.54	–
Basaltic greenstones	14	0.00–0.06	0.00–0.04	0.08
Ultramafics/schists	10	0.01–3.30	0.10–5.30	450.0
Dolerites	15	0.01–0.28	0.00–0.20	–
Amphibolites	11	0.00–0.60	–	0.47

to help achieve this objective; they provide additional depth information. Further, standard 3D Euler deconvolution techniques (Reid et al. 1990) and 2½D magnetic and gravity modelling of selected units (Mushayandebvu 1995; Ranganai 1995, 2012, 2013; Ranganai et al. 2008) give additional depth information to constrain the structural interpretation. The former calculates from the magnetic gradients in the *x*-, *y*-, and *z*-direction the boundary of a magnetic unit and the depth to the boundary (Reid et al. 1990), thus fully locating the unit. Palaeomagnetic data (e.g. Jones et al. 1975, 1995; Mushayandebvu et al. 1994, 1995) and susceptibility measurements (e.g. Table 2, Ranganai 1995) are also used to further constrain the geological interpretation.

Geological interpretation

Interpretation and forward modelling of aeromagnetic data (and other potential field data sets) can be used to determine the large-scale structural orientation, overprinting relationships, and three-dimensional geometry, and allows extrapolation of structural observations to regions that are buried beneath cover sequences (e.g. Gibson and Millegan 1998; Betts et al. 2003). The main focus here is on improving the regional geological mapping and structural information of the area, and therefore, we aim to correlate geologic trends and stratigraphy, and rock units, with magnetic anomaly trends and character. However, more detail is given for those individual anomalies which have a bearing on crustal structure and tectonics. It is worth noting that magnetic maps sometimes highlight outcrop features which are not apparent on geological maps (e.g. Clark and Emerson 1991; Clark 1997). In general, the aeromagnetic data correlate well with geological units: the shapes are clearly outlined, and broad lithological boundaries are discernible (e.g. Figs. 2, 3). Equally, new information is portrayed: several dykes and faults that were not mapped geologically are now indicated (cf. Figs. 2, 3, 4) and will be discussed below.

Lithological units

We mainly use the RTP magnetic data (Fig. 3) and apparent susceptibility map (Fig. 4) for the following interpretation and discussion. Both data sets trace magnetic rock units beneath covered areas, mainly weathered material here, to reveal the shape of subsurface magnetic bodies, and permit extrapolation of lithotectonic features from known outcrops. In the latter (Fig. 4), a regional field has been removed, and the data are downward continued to the surface.

The RTP magnetic data (Fig. 3) display a considerable range of wavelength and amplitude variations but are dominated by high-amplitude, short-wavelength anomalies from shallow sources. For example, several linear anomalies, some coincident with causative known geological features, are seen superimposed on a large regional positive anomaly over the northern parts of the area (Fig. 3). Here, obvious linear magnetic highs occur over the Great Dyke and its satellites (Umvimeela and East dykes; UD and ED), and over ultramafic intrusions (e.g. Ma, Fig. 3), where they map these features very well. The highest observed apparent susceptibilities also occur in this area (Fig. 4), and over the mafic and ultramafic units, iron formations, and over granulite gneisses, with most values broadly in agreement with the measured susceptibilities in the study area (Table 2; Ranganai 1995). Some gneisses contain the mafic minerals biotite and hornblende (e.g. Martin 1978), and this would explain some of the few high susceptibilities obtained from these rocks, while mafic rocks that contain variable amounts of Fe (paramagnetic minerals biotite, amphibolite, pyroxene, and olivine; Clark 1997) also have relatively high susceptibilities. It is worth noting that natural remanent intensities for a few samples were found to be very low, except for ultramafic schists (Ranganai 1995), and therefore their contributions to the anomalies are insignificant. Typical values of susceptibilities for representative rock types are provided by Carmichael (1982). In general, mafic rocks are more magnetic than silicic rocks, and extrusive

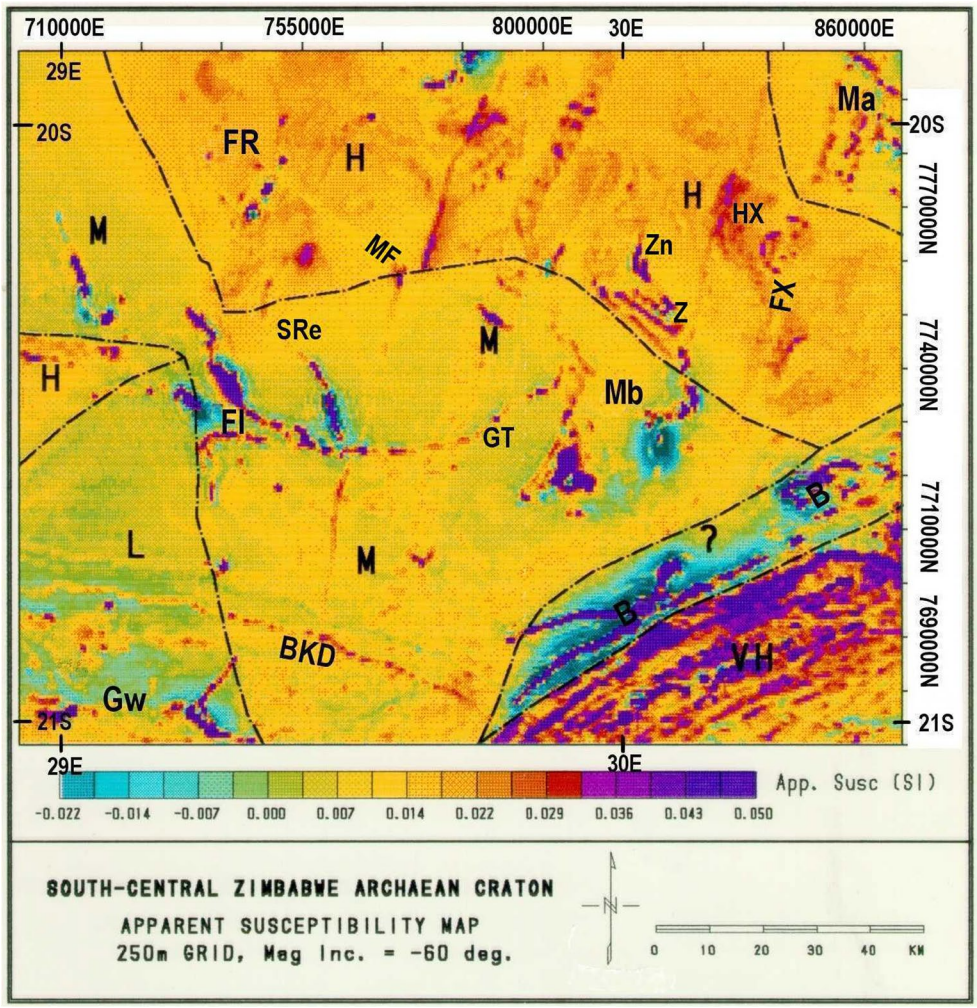

Fig. 4 Apparent susceptibility map of study area also showing different magnetic zones discussed in text. Greenstone belt labels/symbols as in Figs. 1 and 2; magnetic zones *L* low signatures; *M* medium, over predominantly late granites; *H* high, encompassing mainly old tonalitic gneisses normally expected to have low values due to weathering, and *VH* very high signatures, over granulitic gneisses of the north marginal zone, Limpopo Belt. Major dykes (e.g. BKD) and ultramafic complexes (e.g. GT) stand out as high susceptibility units

rocks have lower susceptibility than intrusive rocks with the same chemical composition. Figure 4 also shows different magnetic zones (H, M, L, and VH) discussed later.

In the south-east corner of the study area, the NMZ granulites have a distinct medium- to long-wavelength magnetic high whose northern margin marks the Limpopo Belt–Zimbabwe **C**raton remarkably well (cf. Figs. 2, 3). The highs over the NMZ reflect the high metamorphic grade (granulite facies) of the area (high-grade rocks generally contain more magnetic minerals than other rocks, typically secondary magnetite?), although banded iron formation (BIF), mafic, and ultramafic rocks also occur as inclusions in the area and could contribute to this. To the north of the NMZ highs are magnetic highs over the Buhwa greenstone belt (B, Fig. 3) and intermediate signatures over the Chivi granite. The Buhwa greenstone belt has high magnetic anomalies due to the magnetite- and haematite-bearing quartzites which dominate the lithologies (Fedo et al. 1995). On the other hand, the ~2.6 Ga Chivi granite and other late (i.e. post-volcanic) granite plutons are generally biotite-rich (e.g. Robertson 1973; Martin 1978), and secondary magnetite can be produced from this accessory mineral (Clark and Emerson 1991; Clark 1997), thereby enhancing the magnetic anomalies over them. With the exception of the Buhwa greenstone belt, all the other greenstone belts (e.g. Gw, Mb on Fig. 3), and particularly the dominant Upper Greenstone basalts, are generally characterised by flat magnetic relief. On the margins of, and within, the greenstones belts, however, intense aeromagnetic anomalies with amplitudes up to thousands of nanoTesla are observed over BIF, komatiite, and ultramafic horizons. They emphasise the shape and/or structure of the greenstone belts. Further, the characteristic association of high magnetic signatures with ultramafic and iron formation horizons within greenstone belts is considered of particular economic significance as these units host asbestos, base metal, and gold deposits (e.g. Ranganai and Mhindu 2003).

A striking correspondence between high magnetic and/or susceptibility values and serpentinites and komatiitic basalts is illustrated by the Filabusi and Mberengwa greenstone belts (Fl and Mb, cf. Figs. 2, 3, 4, 5). In the former (Filabusi), there is a clear extension of the ultramafic Shamba Range in a NW to N and then NNE direction

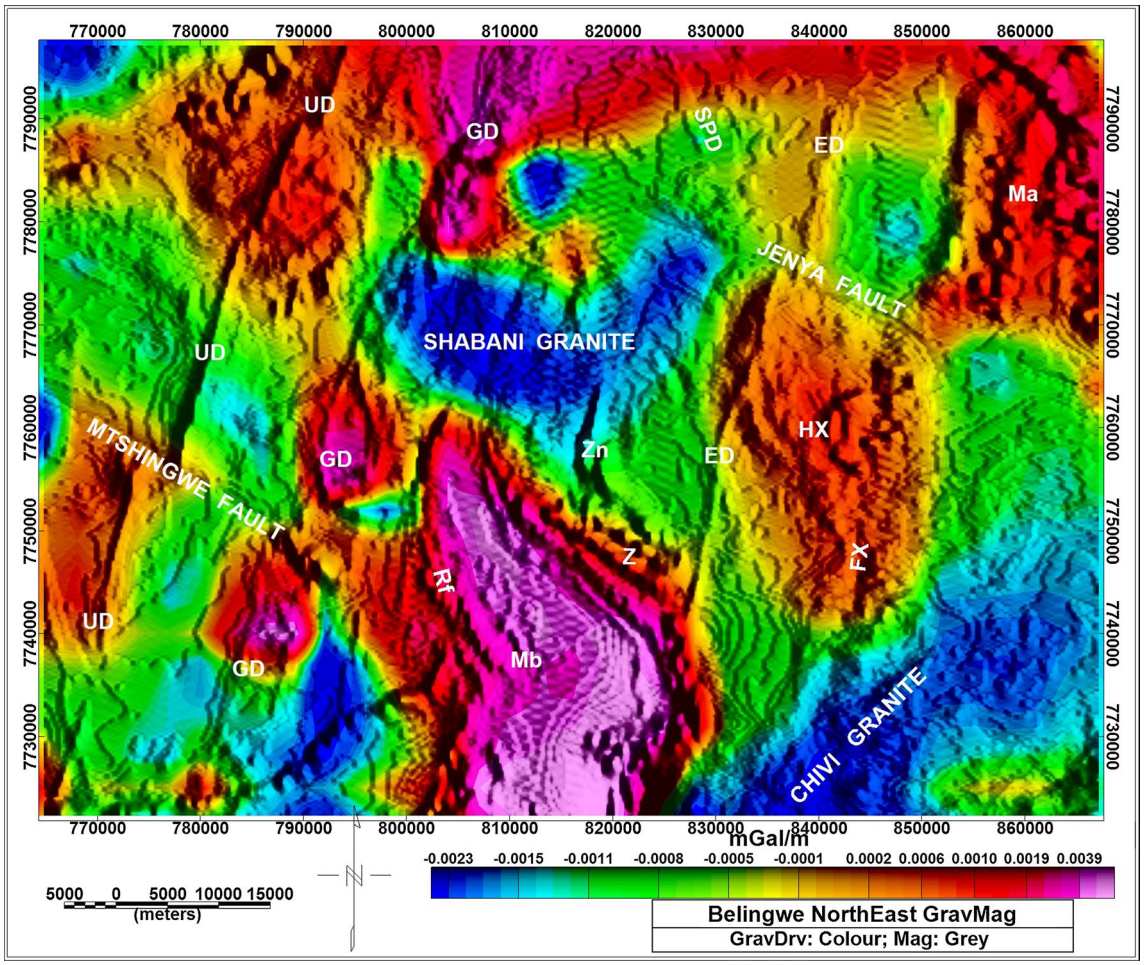

Fig. 5 Reduced to the pole (*RTP*) aeromagnetic data/map of north-eastern part of study area; northern part of the Mberengwa greenstone belt. Note the magnetic highs over the Great Dyke and its satellites (*UD* and *ED*), and over ultramafic intrusions (e.g. *Ma*, *Z*, *Zn*, *S*, and *GT*), where they map these features very well (cf. Fig. 1). Known faults such as the Mchingwe and Jenya appear as narrow zones of low magnetic signature and as breaks or displacements of magnetic zones and/or anomalies. There is also a striking correspondence between high magnetic values and komatiites/komatiitic basalts (Rf- Reliance formation) virtually marking the edges of the Ngezi Group (Upper Greenstones) which dominate the greenstone belt

(SRe, Figs. 3, 4), and mapping of the Gurumba Tumba ultramafic (GT) that in part forms the synclinal axis of the belt. In the latter (Mberengwa), magnetic highs over the Reliance formation (Rf, Figs. 3, 5) of komatiites and komatiitic basalts (Martin 1978; Bickle and Nisbet 1993) indicate the edges of the Upper Greenstones, a stratigraphic (magnetite-rich?) marker horizon. To the immediate north-east of Mberengwa, the Zvishavane ultramafic complex (Z) is clearly mapped, including a previously unknown (e.g. Bickle and Nisbet 1993) northern member or extension (Zn, Figs. 3, 4, 5). Within the adjacent area to the east, an oval-to-rectangular anomaly (HX, Figs. 3, 4, 5) represents another new magnetic body, partly bound to the west and north by the East dyke and Jenya fault, respectively. A coincident gravity anomaly high and proximity to Mashava (Ma) and Zvishavane (Z) ultramafic bodies points to a probable ultramafic composition for the anomaly source (Ranganai et al. 2008). Alternatively, this could be a remnant of the Sebakwe greenstones within the Tokwe segment gneisses (cf Figs. 2, 3). Two previously unknown arms/branches of the Mashava ultramafic complex (Ma) are also identified/indicated (Figs. 3, 4, 5). The high magnetic responses from all the ultramafic rocks could be due to serpentinisation which is common in the area (Martin 1978), and a process which invariably increases magnetite content (Moody 1976).

Over the other units and features, known faults such as the Mchingwe and Jenya commonly appear as narrow zones of low magnetic signature and as breaks or displacements of magnetic zones and/or anomalies (Figs. 2, 3, 5; cf. Ranganai and Ebinger 2008; Ranganai 2013). The faults have increased anomaly values where they cut dykes and

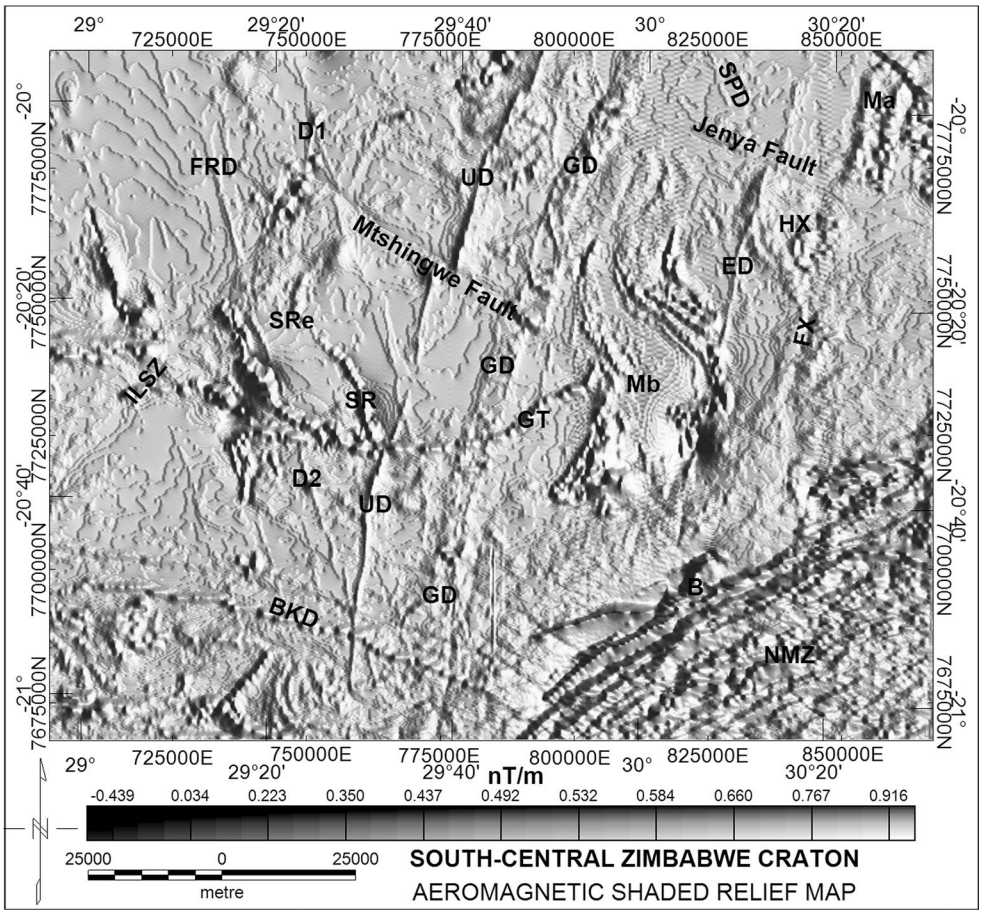

Fig. 6 Shaded relief magnetic map; 'Sun' illumination angle is 30°, declination angles are 60°, 115°. Note the use of two declination angles in order to display the magnetic data which reflect structures at many orientations. *D1*, *D2* dykes discussed in text. Note the dominant *NNW* (*FRD*), *NNE* (Great Dyke), and *WNW* (Mchingwe fault) structural directions

other units (e.g. UD and Great Dyke, Figs. 3, 4), probably due to the introduction of magnetic minerals by hydrothermal fluids. Although some known mafic dykes such as the Umvimeela and East dykes produce obvious high magnetic signatures (UD and ED on Figs. 3, 4), others like the Mashava-Chivi dykes (MCD, Fig. 3) are not clearly magnetically mapped, partly because they fall within a generally high magnetic zone and/or they are too narrow. They are also in places (semi-)parallel to the E–W flight direction (and therefore would not be expected to be magnetically visible), but could also be non-magnetic or weakly magnetic, depending on their precise composition. Such dykes usually turn out to be tholeiitic in composition (Schwarz et al. 1987) with a high content of (non-magnetic) silica, which on the other hand makes them resistant to erosion, and therefore easily mapable in the field and/or on satellite imagery. Stubbs et al. (1999) and Stubbs (2000) suggest that most of these dykes and sills have a close chemical similarity to the continental tholeiitic Mashonaland sills. There is in general an inverse relationship between the silica and magnetite contents of rocks (Clark and Emerson 1991), so that tholeiitic diabase dykes generally contain less magnetite and thus have a lower magnetisation and consequently more subdued magnetic expression than the olivine-bearing variety (Schwarz et al. 1987). Conversely, dykes that have a magnetic expression but are not mapped in the field may be olivine-bearing and tend to weather easily, forming linear depressions filled with overburden (Schwarz et al. 1987), making them invisible during field mapping. However, combined AM and TM images are able to identify such dykes (e.g. Mekonnen 2004; Ranganai and Ebinger 2008).

In general, known dykes appear as linear magnetic highs while faults are low-magnetic zones, as normally expected, and therefore, these signatures are used to map new dykes and faults. For example, a possible fault (FX, Figs. 3, 4, 5) is identified in the north-east of the area, trending NNE parallel to the east dyke (ED). It parallels the Great Dyke trend and cuts across and displaces the eastern part of the interpreted ultramafic body (HX, Figs. 3, 5). This fault also appears to cut the Sebanga Poort dyke (SPD) and some of the Mashava-Chivi dykes (MCD) (cf Figs. 2, 3). It could be part of the Great Dyke fracture system (Wilson 1990), although the observed sinistral displacement is not seen on other fractures. If so, the displacement suggests that the fault may have been locally reactivated. A few WNW–ESE-trending linear anomalies (BKD, Figs. 3, 4) north of the Gwanda (Gw) greenstone belt may be dykes, representing

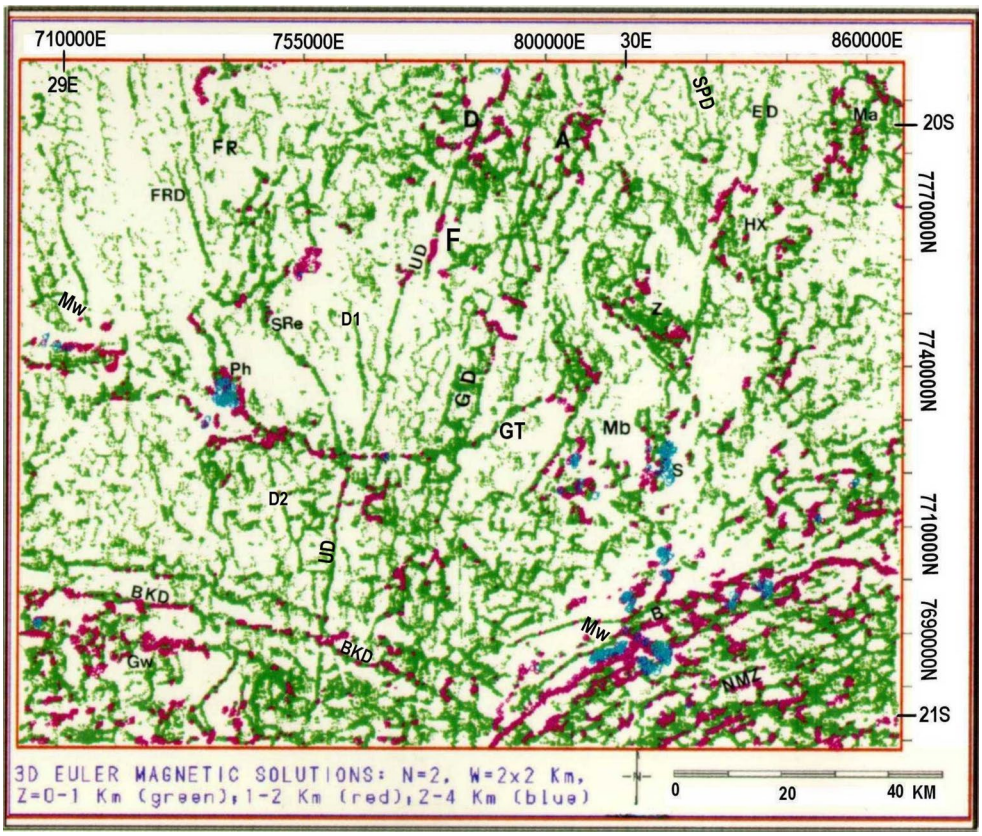

Fig. 7 Euler deconvolution solution map for RTP magnetic grid; $N = 2$, $W = 8$ (2×2 km). Solution depths (Z): *red* = 0–1 km, *green* = 1–2 km, and *blue* = 2–3.5 km. Solution acceptance level set at 70 %. Features and/or trends discussed in text are labelled; *Mw–Mw* Mwenezi fault, *S* Sabi ultramafic complex/unit

a new trend in the area. These and other features are mostly short-wavelength, medium- to low-amplitude anomalies that have been accentuated by the pseudo-relief shading process (Fig. 6) as discussed below.

Structural features

There is a strong unity of objectives between aeromagnetic analysis and structural geology (Betts et al. 2003, 2007; Verduzco et al. 2004). Magnetic studies can help locate faults and dykes or their contacts and reveal their dip and configuration beneath the surface (e.g. Hansen and deRidder 2006; Aitken and Betts 2009). Various data enhancement techniques were applied to generate images useful for interpretation of lineations, textures, and shapes in terms of their geological sources. For example, shaded relief imaging treats magnetic anomalies as topography illuminated from different directions, thus highlighting some of the finer details perpendicular to the illumination direction (e.g. Broome 1990; Cooper and Cowan 2007; Fig. 6). The application of Euler's homogeneity relation through the process of deconvolution has been demonstrated to be an effective method for delineation of potential field boundaries and the estimation of depth to their upper edges (e.g. Reid et al. 1990; McDonald et al. 1992; Ranganai 2012). Euler deconvolution solutions (Fig. 7) provide both structure and depth information and are less subjective than shaded relief maps. However, it should be noted that the depth estimates provided by this method are inherently less well determined than the lateral positional estimates (e.g. McDonald et al. 1992). Using the calibration of magnetic signatures and geological units developed above, these maps reveal several previously unmapped faults and dykes and their extensions, as discussed below.

Structural interpretations are made based on the following assumptions (Nabighian et al. 2005; Aitken et al. 2008; Aitken and Betts 2009; Stewart et al. 2009): (1) short-wavelength aeromagnetic anomalies are the product of lithological contrasts within the shallow crust; therefore, (2) linear aeromagnetic fabrics are the products of deformation on horizontal axes (e.g. shortening, tilting, folding or faulting of a stratigraphic package with internal magnetic contrasts) or deformation such as extension and the emplacement of dykes; (3) truncations or displacement of magnetic anomalies and/or juxtaposition of regions with different magnetic character indicate the location of a fault or shear zone; (4) rotation or offset of marker anomalies indicates the apparent strike-slip separation; (5) folds can be mapped and interpreted where a series of magnetic horizons are repeated or by identifying the fold axis, and (6) gradients within the potential field data sets can serve as a proxy for

the dip direction of sources to magnetic (if remanence is small) and gravity anomalies whereby, with respect to a single linear anomaly, the side with the shallower gradient indicates the direction of dip (see Hansen and deRidder 2006). From these structural elements, the overprinting relationships between deformation events can be inferred using techniques similar to those in structural geology (Betts et al. 2007; Aitken and Betts 2009). However, caution should be exercised where there is no direct structural and/or lithological constraints (Aitken et al. 2008).

The shaded relief and Euler deconvolution solution maps (Figs. 6, 7) are marked by conspicuous NE, NNE, NNW, WNW, and NW anomaly trends; lineaments; and breaks in the anomaly pattern, most parallel to geological trends (Fig. 2) or with a direct coincidence of linear clustering solutions. Most of these correspond to known features such as the Great Dyke and its satellites, the FRD group, and the Mchingwe and Jenya faults, respectively (Figs. 2, 3, 4, 5) (as above). A distinct linear cluster of solutions with depths around 2.0 km (Fig. 7) marks the Zimbabwe **C**raton–Limpopo Belt boundary, providing supporting evidence that the boundary previously defined by the orthopyroxene isograd is a tectonic break/contact. The Great Dyke and its satellites, the Umvimeela and East dykes, or at least the faults (marked by magnetic lows) which they intruded, appear to extend beyond their mapped exposures into the NMZ of the Limpopo Belt (Figs. 6, 7). The widths of these known features are also represented well on the Euler solution maps, particularly at small structural indices where, for example, both edges of dykes are clear (cf Figs. 2, 6, 7). It is worth noting that most features are sub-vertical, as confirmed by the zero vertical gravity gradient coincident with the edges as well as symmetric horizontal derivatives (Ranganai 1995; Ranganai et al. 2008). Some linear solutions can be traced for distances from tens of kilometres to just over 100 kilometres (e.g. UD, FRD, BKD; Fig. 7), but others are broken up into segments. The latter are best viewed on printed large-scale maps and/or 'on-screen' displays with higher resolution than figures presented, allowing their identification as continuous trends and/or significant structures of considerable strike. The Euler solutions map (Fig. 7) also suggests that the Mwenezi fault (Mw F, Figs. 2, 6) can be extended in both directions from the mapped exposure to cut across the entire study area and into the Limpopo Belt in the south-east (Mw–Mw, Fig. 7). Other anomalies are much shorter, but the various segments form part of more continuous features; faults can be interpreted at these breaks, but the longer breaks may represent zones of constant susceptibility.

The shaded relief and Euler deconvolution solution maps (Figs. 6, 7) also reveal conspicuous NNW anomaly trends, associated with Proterozoic dykes outcropping west of Fort Rixon (FRD, D1, D2, Figs. 2, 3, 6). Their clear signatures show that the dykes are more continuous than mapped on the surface, extending to south of the Filabusi greenstone belt (Fl) (e.g. D2). The one mapped east of Filabusi (D1, Figs. 3, 6) can be seen extending continuously northwards east of, and beyond, the Fort Rixon (FR) greenstone belt. Here, it is cut by the Mchingwe fault but without any obvious displacement, providing a relative age constraint for all the associated NNW-trending dykes (see below). The NNW trend also appears as drainage lineaments and/or as dense vegetation lines on Landsat TM images (Ranganai and Ebinger 2008). The extension of this swarm can also be traced into the NMZ where it has been referred to as the Crytsal Springs swarm (Robertson 1973; Wilson et al. 1987). Other new features and strike directions now readily apparent include the WNW–ESE-trending linear anomalies in the south-west, north of the Gwanda greenstone belt (Gw) (BKD, Figs. 3, 4), extending from west of the study area and cutting through the granitic terrain into the NMZ (BKD, Figs. 6, 7). Although mafic dykes are known to cause positive and occasionally negative magnetic anomalies with respect to most host rocks (e.g. Schwarz et al. 1987), the change in appearance (magnetic signature) within the BKD swarm (Figs. 3, 4, 6) suggests some are reversely magnetised. This swarm clearly cuts the Filabusi–Fort Rixon dykes (FRD) and truncates all other magnetic structures in the area, and may have been intruded in several episodes spanning a magnetic reversal (Halls and Fahrig 1987; Reeves 1989; Clark and Emerson 1991; Clark 1997).

Similarly, some newly identified and/or confirmed structures of tectonic significance include an >3 km wide NE-trending linear magnetic zone (ILSZ, Fig. 6) west of Filabusi and south-east of Fort Rixon. This correlates with the Irisvale–Lancaster shear zone (ILSZ, Fig. 2) which was previously partly mapped from field observations, air photographs, and Landsat MSS data (Stowe 1980; Wilson 1990; Campbell et al. 1992). It is envisaged that the Fort Rixon greenstone belt separated from the Bulawayo–Filabusi greenstone belt along this shear zone, accompanying the intrusion of ~2.7 Ga syn-volcanic granite plutons (see Fig. 2; Stowe 1980; Wilson 1990). Significantly, the ILSZ coincides with a 'break' in the gravity gradient between the Filabusi and Bulawayo greenstone belts (Ranganai 1995, 2013; Ranganai et al. 2008; see below). On the other hand, the Shamba range extension north of Filabusi (SRe, Figs. 3, 6, 7) appears to swing from NW to N and then NNE at or near the shear zone south-east of the Fort Rixon greenstone belt, providing apparent dextral kinematics along the shear zones. This may be consistent with the theory (Wilson 1990; Wilson et al. 1995) that the Fort Rixon greenstone belt was detached from the Bulawayo–Filabusi greenstone belts as this parallels the direction of movement along the ILSZ. These kinematics are partly

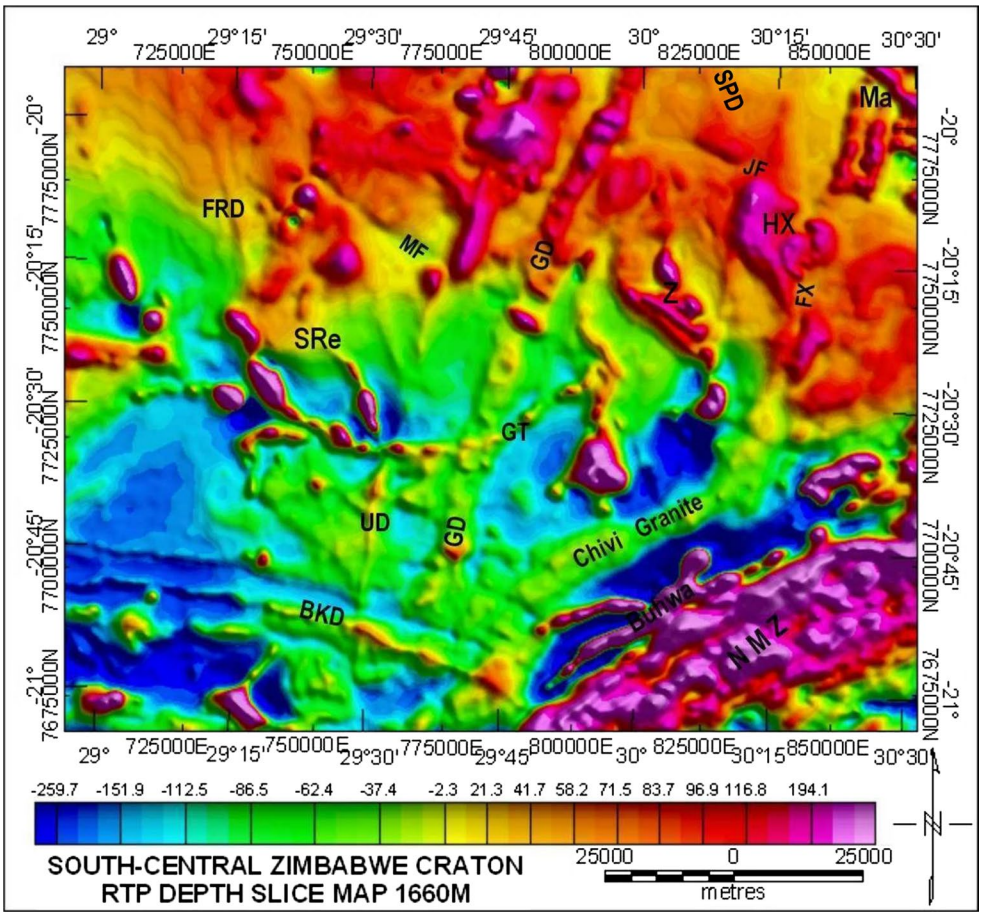

Fig. 8 Matched bandpass filtered anomaly map from the RTP aeromagnetic data corresponding to a depth slice of ~1660 m showing regional features. Geological unit labels are for reference purposes (cf Figs. 2, 3, 7); responses from most geological units have disappeared. Note that a good range of wavelength still exists, but intermediate wavelength features are enhanced

confirmed by ~15 km of apparent offset of the Fort Rixon and Filabusi ultramafic complexes (Fig. 2). Up till recently (Ranganai 2013; this study), the existence and location of this important shear zone have not been confirmed using geophysical methods.

Magnetic zones as crustal domains

Based on the grid power spectra (e.g. Spector and Grant 1970; Talwani et al. 2003), shallow and deep depth slices of the magnetic field were able to separate the high-frequency anomalies from the low-frequency ones. Figure 8 shows the filtered RTP magnetic data due to a depth slice of ~1600 m (corresponding to a layer with a maximum depth of 1.3 km) where several high-frequency anomalies are now absent on the filtered magnetic map, indicating that their sources lie in the top ~1000 m. However, most major faults, greenstone belts, and mafic–ultramafic horizons are still present on this map, which implies that they are deep crustal structures; mafic–ultramafic intrusives are signs of deeply rooted magma (e.g. Bauer et al. 2003; Ferraccioli et al. 2005; Allek and Hamoudi 2008). Greenstone belt depths range from 3 to 6 km (Ranganai 1995, 2013; Ranganai et al. 2008); therefore, their magnetic effects are still present. The map is easily divided into three zones/segments: northern area with high values (mostly red), south-east corner of NMZ highs (purple), and the remaining central and western parts with low values (green/blue). The south-western corner could be considered a fourth zone of very low values (Fig. 8). Generally, delineating areas of magnetic anomalies having similar characteristics isolates areas of crust having similar lithological, metamorphic, and structural character and, possibly, history (Teskey and Hood 1991; Gibson and Millegan 1998; Nabighian et al. 2005). However, the continuity of intrusive bodies and structures across sub-domain boundaries (e.g. GD, UD, Fig. 8) implies that horizontal and vertical offsets are not extreme, the sub-domains were assembled prior to development of cross-cutting lineations, and that the adjacent sub-domains can be expected to have a largely shared structural evolution (Aitken and Betts 2009). Interestingly, juxtapositioning of such multiple (distinct) lithotectonic terranes along regional-scale structures has been used as evidence for allochthonous accretion, and the operation of plate tectonics in the craton since the Paleoarchaean (Dirks and Jelsma 1998, 2002; Kusky 1998; Jelsma and Dirks 2002).

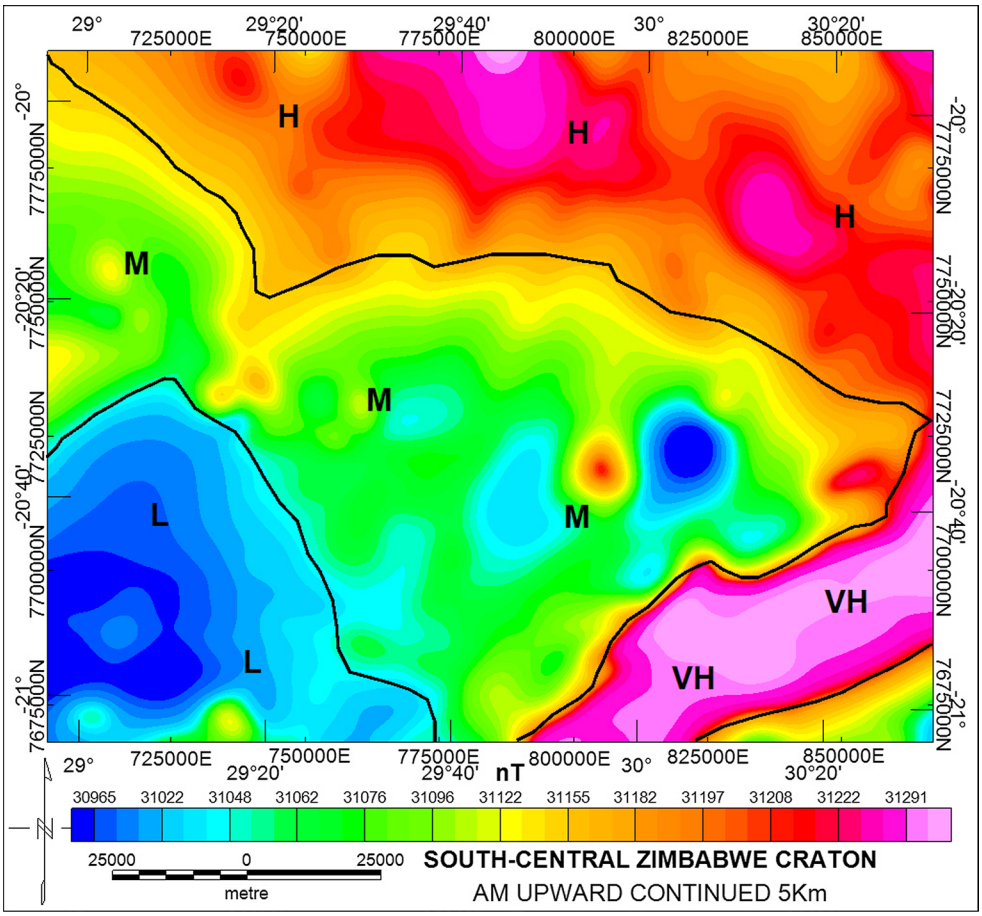

Fig. 9 Aeromagnetic map upward continued to 5 km and identifying large-scale magnetic zones (*L* low; *M* medium, *H* high, and *VH* very high signatures) as deep crustal features (cf Fig. 2); magnetic effects of *shallow* (surface and near-surface) geological units have all virtually disappeared

Upward continuation was also performed on the RTP magnetic grid to remove the effects of shallow sources while preserving the regional anomalies that reflect basement magnetic zones and deeper crustal structures than those discussed above (e.g. Teskey and Hood 1991; Blakely 1995; Ferraccioli et al. 2005). The results for a continuation height of 5 km (20 grid cells, average depth extent of greenstone belts) are presented in Fig. 9. Magnetic effects of surface and near-surface geologic units are now virtually absent, except for the interpreted ultramafic body (HX). Persistent occurrence of this magnetic anomaly on the upward continued data (Fig. 9) indicates that the body extends to great depths, thus precluding the possibility of Sebakwian greenstone inclusions as anomaly sources. Four distinct crustal blocks (L, M, H, and VH) are clearly defined (see also Fig. 8), and each encompasses several different surface geological units (cf. Fig. 2), suggesting that they are fundamental basement or magneto–tectonic provinces. They can also be identified on the RTP map (Fig. 3) and apparent susceptibility map (Fig. 4) based on anomaly textures, defined by parameters such as linearity, relief, and background level, and features such as anomaly shapes and wavelengths (e.g. Stettler et al. 1989).

In general, it is difficult to relate the crustal (sub-) domains to known geological events, structures, and units exposed at the surface, and their significance is not yet clear. For example, the zone of high magnetic and apparent susceptibility values (H) encompasses various lithologies and units in the northern part of the study area, including gneisses, tonalites, and granites of different ages, as well as mafic–ultramafic bodies. However, this zone appears to be a separate terrain mostly over the ~3.5 Ga older gneisses, partly bounded by the dextral Mchingwe and Jenya faults and/or other structural breaks (see Figs. 2, 3, 4). The southern margin/boundary of the zone partly coincides with the zero contour of residual gravity (Ranganai 1995; Ranganai et al. 2008). It is highly probable that the increase in the 'background' magnetic susceptibility over the gneisses and tonalites reflects a higher grade of metamorphism (cf Clark 1997). Significantly, the 'snake head'-shaped section of the Mberengwa greenstone belt in this area (Sh on Figs. 2, 3, 5) is reported to be at higher grade (amphibolite facies) than the main belt (greenschist facies), and probably from deeper crustal levels (Martin 1978; Bickle and Nisbet 1993). Based on magnetic modelling and palaeomagnetic data from the Umvimeela and East dykes, Mushayandebvu (1995) suggests a tilting of the craton adjacent

to the Limpopo Belt, the affected block being limited by the cross-cutting Mchingwe fault, parts of which form the approximate boundary of the magnetic zones. We infer that zone H underwent at least one major period of heating and relative uplift, followed by erosion. This is quite possible since the mechanism of transpression allows relatively small pieces of fault-bounded crust to be displaced upwards or downwards while adjacent blocks remain static (e.g. Belton and Raab 2010).

Zone M is characterised by medium-amplitude magnetic intensities and apparent susceptibilities in the south-centre of the area, between and including Mberengwa (Mb) and Filabusi (Fl), occurring mainly over granitic terrain (Figs. 2, 4, 9). In general, the zone appears to cover some of the gneisses and most of the late granites, but some dykes and ultramafics stand out as high-amplitude, short-wavelength linear to curvilinear anomalies. Within this moderately magnetic zone are small areas of low magnetic signatures. Broadly following this to the west is zone L, a relatively small area of low-magnetic values to the west of Filabusi down to and including the Gwanda greenstone belt (Gw) in the south-west (Figs. 4, 9). Distinctive very high anomalies, zone VH, partly over the Buhwa greenstone belt (B) but mainly due to the NMZ granulites, clearly mark the Zimbabwe **C**raton–Limpopo Belt boundary in the south-eastern corner of the area (Figs. 3, 4, 8, 9). A similar situation is reported between the Limpopo Belt (SMZ) and the Kaapvaal Craton in South Africa (Stettler et al. 1989). Similarly, Percival and West (1994) report local intense aeromagnetic anomalies and broad regional highs over various lithotectonic elements of the Kapuskasing uplift, which is generally made up of high-grade metamorphic rocks. The well-defined magnetic boundary and the 3D Euler deconvolution solutions together support the interpretation of the contact as a tectonic break (North Limpopo Thrust Zone, NLTZ), separating a shallow crustal domain (the craton) from a deep crustal (NMZ) thick-skinned domain (cf. Mkweli and Dirks 1997).

It is worth noting that although the magnetic zones can be identified on the RTP and apparent susceptibility maps, they are not represented in any recognisable pattern on the Euler solution maps at all structural indices (e.g. Fig. 7). This partly confirms the interpretation that the zones reflect relatively deep crustal blocks, whereas the maximum depths obtained from Euler deconvolution rarely exceeded 2.5 km (Ranganai 1995, 2012).

Regional structures and their tectonic significance

The derivatives, shaded relief images, and Euler deconvolution solution maps on which lineaments, discontinuities and displacements are clear were able to map upper crustal structures (e.g. Figs. 6, 7), while pseudo-depth slices (Fig. 8) showed intermediate source ensembles. Another informative presentation shown here is a combined magnetic shadow and gravity colour raster map (Figs. 5, 10), to portray both shallow- and intermediate-depth structures. This is based on the fact that an RTP map is expected to correlate directly with the vertical gravity gradient map when both anomalies arise from a common source (Poisson's relation, e.g. Blakely 1995). Examples in this regard are the various ultramafic bodies, including the Great Dyke and a concealed body, HX (Figs. 2, 5, 6, 8, 10). The gravity reflects relatively deep crustal features and is characterised by Bouguer gravity anomaly highs over the greenstone belts and ultramafic bodies (Mb, Fl, FR, GD), and lows over granite plutons (Chivi granite, N, Sg). Gravity data interpretation shows that the anomalies are due to geological units in the upper 8–10 km of the crust (Ranganai et al. 2008). An interesting new feature identified on this map is a WSW–ENE- to W–E-trending anomaly cutting across the north-central part of the study area (WE, Figs. 3, 10). This structure is subdued on the separate data sets, but here it in part marks the boundary between distinct gravity and magnetic terrains (e.g. Shabani granite gravity low, Sg, Fig. 10; Ranganai 1995; Ranganai et al. 2008). In the west, it terminates at the NE–SW-striking Irisvale–Lancaster shear zone (ILSZ), on the northern end of the Shamba range extension (SRe, Fig. 10) south-east of the Fort Rixon greenstone belt. Thus, the combined interpretation of the gravity and enhanced aeromagnetic image allowed subtle anomaly patterns to be identified and traced with much greater certainty than in one data set alone.

The final structural interpretation map (Fig. 11) was guided by printed colour maps at various scales and 'on-screen' displays with higher resolution than figures presented. Figure 11 is a compilation of (a) known structures, (b) anomalies calibrated by surface geology, and (c) structures interpreted by analogy to (b). The deformation nomenclature (Table 3; Fig. 11) follows that of Aitken et al. (2008) denoting the relevant data sets: $D^{S}X$ (structural interpretation), $D^{M}X$ (magnetic interpretation), $D^{L}X$ (Landsat TM interpretation), and DX (combined interpretation). The regional distribution of the lineaments and their overall magnetic character (e.g. Figs. 3, 4, 5, 6) plus gravity and geological evidence suggest that the lineaments are major structural features in the basement rocks.

Generally, the western half of the study area is characterised by NNW-trending structures, in places cut by NW-trending faults, whereas the east is dominated by NNE-trending structures, in places cut by NW-trending faults and NNW-trending dykes (e.g. Figs. 3, 6, 7, 10, 11). E–W- to WNW–ESE-trending dykes in the south-western corner occur with both normal magnetisation and reverse magnetisation, implying multiple episodes of intrusion. Some of

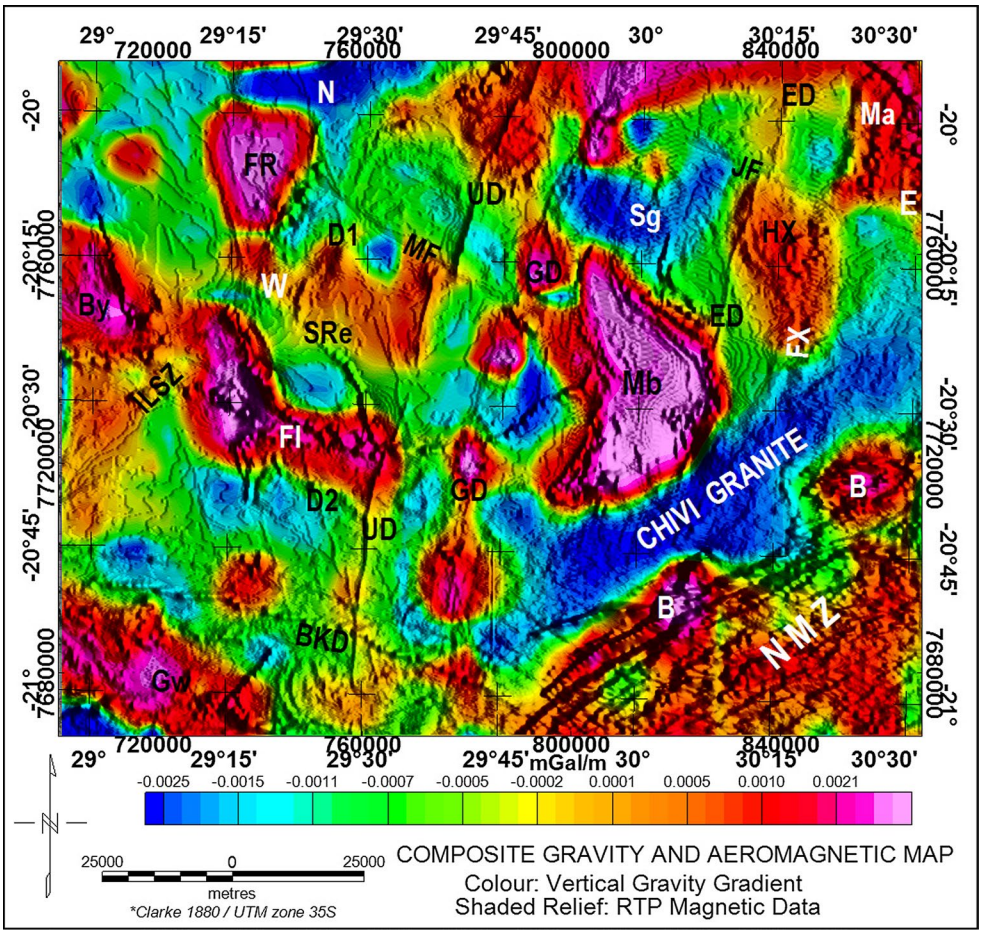

Fig. 10 Combined aeromagnetic *shadow* and gravity gradient colour raster map. Illumination angle is 30°; declination angles are 60°, 115° (two declination angles are used to enhance structures at many orientations). See previous figures for unit labels. Note coincidence of magnetic structure *WE* with margins of gravity lows (e.g. *Sg*), and *stratigraphic folds* visible in Mberengwa (*Mb*) greenstone belt

these dykes form the eastern extension of the >1000-km-long Late Karoo Dyke Swarm that has been mapped across northern Botswana (cf. Wilson et al. 1987; Reeves 2000; Le Gall et al. 2005). These may constitute a failed third arm of a rift triple junction associated with the break-up of Gondwana, with the Sabi and Lebombo monoclines forming the other two arms (Reeves 2000).

Overall, five major structural trends (regional lineaments) can be identified and associated with the various geological features and craton tectonic events as summarised in Table 3 (cf. Fig. 11), based on previous studies and cross-cutting structures. Relative ages of the structures can be inferred from the details of the intersection relationships and other geochronological information (e.g. Taylor et al. 1991; Mushayandebvu et al. 1995). However, it has not been possible to associate some of the interpreted structures with the known or postulated geological units and events. For example, the apparently deep ENE- to WE-trending structure in the central part of the area (W–E, Figs. 10, 11) has no obvious geological significance, although it is in places coincident with the Jenya fault and pluton edges (Fig. 10; Ranganai 1995). On the other hand, the NNW-striking FRD dykes have been previously correlated with the Sebanga dyke (SPD, Figs. 2, 5, 6, e.g. Wilson et al. 1987), but the lack of displacement on the former (along the Mchingwe fault) suggests that they are younger (see discussion; cf Söderlund et al. 2010). They are also not cut by the W–E structure, whereas the SPD is discontinuous and displaced in this area and elsewhere. Alternatively, it may imply that movement (probably reactivation) on the fault was limited/confined to the east.

Using the various Euler solution maps (not shown), the magnetic sources in the northern parts of the area (north of latitude 20.5°S or UTM 7740 000N; Fig. 7) generally appear shallower than in the southern parts by up to 500 m (Ranganai 1995, 2012). This suggests that either the sources were emplaced at shallow levels or that the north experienced more uplift and higher erosion levels than the south since Proterozoic time. The latter interpretation is supported by the fact that the northern part of the Mberengwa (Belingwe) greenstone belt is considered to be a deeper level crustal section than the main belt to the south (Martin 1978; Bickle and Nisbet 1993). Since Cretaceous time, Belton and Raab (2010) use apatite fission-track thermochronology (AFTT) analyses to document a south-to-north decrease in exhumation, suggesting that the difference in structural levels across

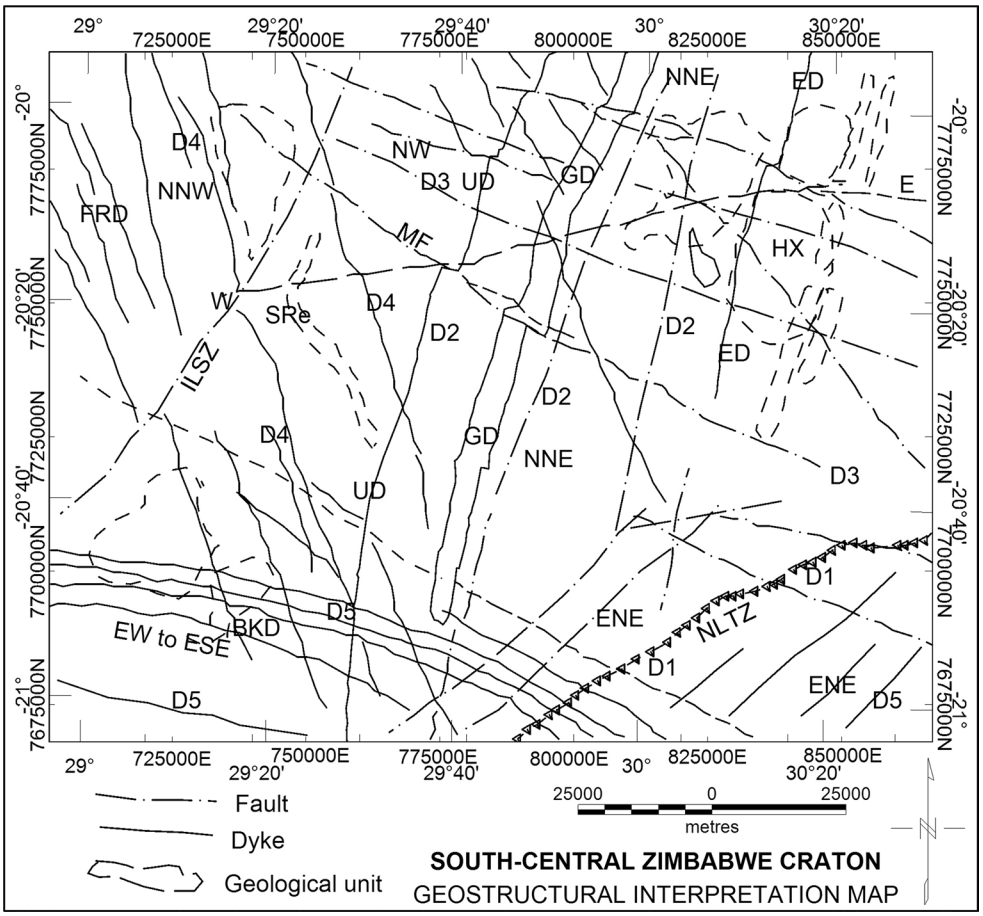

Fig. 11 Geological and structural interpretation map of the study area based on gravity and magnetic data (see Fig. 2; Table 3 for comparison). Structural features: *GD* Great Dyke; *MF* Mtshingwe fault; *NLTZ* North Limpopo Thrust Zone, other labels as in Fig. 2; *ENE*, *EW* to *ESE*, *NNE*, *NNW*, and *NW* labels refer to general trends of the features and structures (see Table 3). *D1–D5* refer to deformation stages as discussed in text

Table 3 Major aeromagnetic structural trends and their geological association. (See Fig. 11)

Trend/direction	Type of feature	Associated geological features/craton tectonic events and timing/age
E–W to ESE–WNW	(D^M5); (D^L4) D5	Botswana Late to post-Karoo dyke swarm, BKD; Plumtree dyke swarm (Gondwana break-up: Reeves 2000; Wilson et al. 1987; Duncan et al. 1997) 170–200 Ma (Extensional event)—**Dilation?**
ENE–WSW	(D^M5); (D^L4) D5	Sabi–Limpopo dyke swarm (Karoo Igneous event; Wilson et al. 1987; Duncan et al. 1997; Jourdan et al. 2006) 170–200 Ma (Extensional event)—**Shear stress**
NOT identified?	Not applicable	Umkondo Igneous event (Wilson 1990; Wilson et al. 1987; Mushayandebvu et al. 1994; Hanson et al. 1998). 1100 Ma (Extensional event)—**Shear stress**
NNW–SSE	(D^M4); (D^S4) D4	Sebanga Poort dyke set, including Filabusi and Fort Rixon dykes, FRD. (Mashonaland Igneous Event: Wilson et al. 1987; Wilson 1990). 1800–2000 Ma (Extensional event)—**Compression?**
NW–SE	(D^M3); (D^S3) D3	Mchingwe–Jenya–Mwenezi faults plus others (Dextral shear couple acting on craton Wilson 1990; Campbell et al. 1992) ~2000 Ma Dextral shear couple acting on craton (**Under compression?**)
NNE–SSW	(D^M2); (D^S2) D2	Great Dyke, East and Umvimeela dyke, plus Popoteke fault set (Great Dyke fracture system: Wilson 1990). 2500 Ma Great Dyke fracture system (**Under shear stress**)
ENE–WSW	(D^M1); (D^S1) D1	NMZ, Chivi–Razi granites, (Limpopo orogeny; LB over thrust onto ZC: Roering et al. 1992; Mkweli et al. 1995; Frei et al. 1999) ~2650–2600 Ma (Collisional event)—**Shear stress**

the southern Zimbabwe **C**raton and Limpopo belt was more pronounced in the past. Similarly, magnetic modelling of profiles in several places across the Umvimeela and East dykes within the study area shows a progressive increase in depth to top of unit/source from north (100 m) to the south (300 m) (Mushayandebvu 1995). However, the Great Dyke and its satellites are seen to have isolated areas having slightly deeper solutions of 1.5–2.0 km within the northern parts of the area. For the Great Dyke, the area of deep solutions (A, Fig. 7) approximately coincides with the boundary of the Wedza and Selukwe complexes (Wilson and Prendergast 1988), but it is not yet possible to place any significance to this. A similar area (D) occurs on the Umvimeela dyke (Fig. 7). On this dyke (UD), another area of deep solutions (F, Fig. 7) just north of the Mchingwe fault correlates with a point interpreted as its possible feeder point, identified through magnetic fabric analysis (Bates and Mushayandebvu 1995).

Spectral analysis results indicate three magnetic susceptibility discontinuities at about 0.6, 2.5, and 8.0 km depths, the first two in agreement with Euler deconvolution results (Ranganai 2012). The 8 km depth maps the magnetic basement, and this probably corresponds to a crustal boundary deduced from gravity (Ranganai 1995; Ranganai et al. 2008) and seismic (unpublished data, R Clark pers. comm. 1995) data, at 9–10 km depth. However, upward continuing the aeromagnetic data to 8.0 km did not yield significant differences to Fig. 9.

Discussion

Structural and tectonic evolution of the region

We consider here the significance of the aeromagnetic anomaly and lineation patterns to other geological events, including any precursory or terminal phenomena associated with the dyking process. The occurrence of mafic dykes indicates periods of heating and lithospheric extension, at times corresponding to their ages (see Halls and Fahrig 1987; Parker et al. 1990; Uken and Watkeys 1997; Le Gall et al. 2005). Additionally, ring dykes (e.g. MCD, Fig. 2) and mafic dykes are the intrusive equivalents of modern rift zones, such as the Main Ethiopian rift above the Afar plume (e.g. Wolfenden et al. 2004). Patterns of the mafic intrusions can be related to regional tectonics affecting the craton; consistent orientations provide constraints on the state of stress at the time of emplacement. Cross-cutting relations suggest that basement structures have been reactivated during later tectonic activity (e.g. Wilson 1990; Campbell et al. 1992; Dirks and Jelsma 1998, 2002). For example, the left-lateral displacements of the Mchingwe and Jenya faults (e.g. Figs. 2, 3) indicate Late Proterozoic–Phanerozoic activity in this part of the craton. These relations are summarised in Table 3, which also gives associated events in the craton. Based on data from the world stress map, Ranganai and Ebinger (2008) assessed the present-day relative shear and compressive stresses for each lineament direction using simple stress resolution diagrams (Table 3).

It is clear from Table 3 that structures mapped are predominantly Late Archaean and Proterozoic in age because they cut across the >2.7 Ga greenstone belts and the 2.5 Ga Great Dyke (e.g. Figs. 5, 6, 7, 8). This is also seen in the north-eastern Kaapvaal Craton where magnetic lineament patterns are not influenced by the presence of the greenstone belts (Stettler et al. 1989). An important implication is that the greenstone belts were an integral part of the lithosphere before much of the upper crustal (brittle?) deformation occurred. Thus, our analyses shed light on Late Archaean (Neoarchaean) to Phanerozoic tectonics, but provide little information on earlier Archaean events, which have been masked by later activities. For instance, the ~3.5 Ga granites are deformed together with the greenstone belts, but these belts are modified by later deformation and younger (~2.6 Ga) intrusive granites which form large irregular shaped batholiths and clearly post-date all the ductile deformation (cf. Figs. 1, 5; Coward et al. 1976; Wilson 1990; Bickle and Nisbet 1993). However, the phenomenon of inherited trends common in the craton (Stowe 1980; Wilson et al. 1987; Wilson 1990; Campbell et al. 1992; Dirks and Jelsma 2002) implies that some of the observed structural orientations mimic the earlier Archaean structures. For example, the strike of NNE and NW dyke and fault directions coincide with the faults linking the limbs of the pre-deformation ~2.7 Ga Mashava ultramafic complex (Ma, Figs. 2, 3, 4, 5) and the NNE–SSW structural trends within the Tokwe segment. It could also be possible that local and regional stress rotations caused by lithospheric-scale heterogeneities control subsequent magma production, transport, and storage.

All the interpreted structures (Fig. 11) seem to converge in the south-centre of the area, around the Zimbabwe **C**raton–NMZ (Limpopo Belt) boundary (see also Fig. 12), suggesting a common origin involving the two terranes (Ranganai 2012), or repeated deformation around the boundary (e.g. Roering et al. 1992; Treloar and Blenkinsop 1995). Throughout the Zimbabwe **C**raton and the Limpopo Belt, there is evidence for regional compression (e.g. folds), and local extension and lithospheric heating (e.g. mafic dyke swarms). For example, the NE-trending elongate form of the intrusive 2.6 Ga Chivi granite (and other related Chilimanzi plutons) may record the northward thrusting of the NMZ onto the Zimbabwe **C**raton at about the same time (Robertson 1973; Mkweli et al. 1995; Frei et al. 1999). The WE structure has this general trend, but the link is not clear although it in part marks the boundary of the Shabani

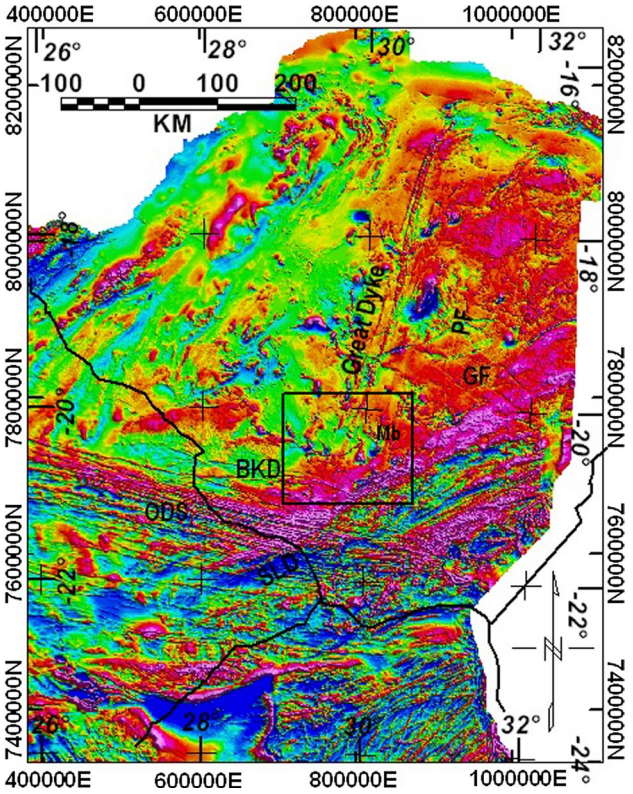

Fig. 12 *Aeromagnetic shaded* relief map of the Zimbabwe **C**raton showing major structural trends and dyke swarms. The Mberengwa greenstone belt (Mb) and the Great Dyke are labelled for reference purposes; *GF* Gutu fault; *PF* Popoteke fault, *SLD* Sabi–Limpopo dyke swarm. Note the different trend of the Botswana Karoo dykes (*BKD*) from that of the main Okavango dyke swarm (*ODS*). The *rectangle* locates the study area (Fig. 2)

granite pluton (Sg, Figs. 2, 8), a correlate of the Chivi granite. Further, there is a general increase in Euler deconvolution solution depths in the area from north to south which may reflect variable uplift and erosion levels between the two halves of the area, with the southern parts having been affected (depressed) by loading of the area by Limpopo Belt rocks thrust onto the southern edge of the craton. The thrusting also resulted in the tilt of the basement (about a horizontal axis) and produced a rotation of the south relative to the north by ~14° (Mushayandebvu 1995). So, given the evidence for differential exhumation from Cretaceous to recent, these effects would have been more pronounced prior to Cretaceous time (Belton and Raab 2010).

Ranganai et al. (2008) have argued that the tectonic evolution and deformation of the greenstone belts in the area between 2.6 and 2.9 Ga involved the intrusion and extrusion of magma within continental rift zones that formed above or near mantle plumes, followed by subsidence and rapid deposition of sediments. The volcano–sedimentary sequences were subsequently deformed by intruding younger plutons and affected by strike-slip activity producing cross-cutting structures. Based on patterns observed on enhanced magnetic maps and supported by gravity, palaeomagnetic, and geochronology, we suggest the following chronology of the magnetic trends from the Late Archaean onwards (the post-volcanic era; Table 3).

The ENE–WSW trend (D1, Fig. 11) is associated with the collision of the Kaapvaal and Zimbabwe **C**ratons (Roering et al. 1992; de Wit et al. 1992; Khoza et al. 2013) during the Neoarchaean (2.7–2.6 Ga) to produce the Limpopo Belt. However, it is also noted that Söderlund et al. (2010) propose the formation of the Kalahari Craton, i.e. continental collision (and amalgamation) of the Zimbabwe and Kaapvaal Cratons, much later at 2.0 Ga. This ENE–WSW trend of the NMZ is also seen on the adjacent Chilimanzi suite granites: the Chivi and Razi plutons (Robertson 1973; Campbell et al. 1992; Fedo et al. 1995; Mkweli et al. 1995; Jelsma et al. 1996; Frei et al. 1999; Gwavava and Ranganai 2009). The youngest swarm of the ~2.7 Ga Mashava-Chivi dykes (MCD; Fig. 2) also shows this ENE trend (Wilson et al. 1987). These points/considerations invalidate the hypothesis of Söderlund et al. (2010).

The NNW–SSE directed crustal shortening due to the NMZ over thrust onto the Zimbabwe **C**raton produced the regionally distributed conjugate sets of NNE-trending sinistral and ESE-trending dextral shears: the Great Dyke fractures (D2, Fig. 11) and the Mchingwe–Jenya fault set (D3, Fig. 11), respectively (e.g. Wilson 1990; Campbell et al. 1992). Many WNW-trending faults (D3, Fig. 11) partly run along the outcrops of 2.6 Ga Chilimanzi suite plutons (e.g. Mchingwe, Ngomi, Fig. 2), and it seems likely that the emplacement of the plutons was broadly coeval with the development of these faults (Campbell and Pitfield 1994). The close spatial association between the Mchingwe fault and the ~2470 Ma Mchingwe dolerite may indicate syn-intrusive faulting (Söderlund et al. 2010). All other structures that predate emplacement of the 2.6 Ga Chilimanzi plutons relate to internal deformation of the craton involving some jostling of crustal blocks (e.g. Coward et al. 1976; Wilson 1990; Treloar and Blenkinsop 1995). The collision ceased around 2570–2580 Ma, and the Great Dyke and its satellites intruded along NNE release fractures; together, they form the first major igneous event after cratonisation (Wilson 1990), marking the onset of a significant phase of crustal extension in the craton (Campbell et al. 1992). They do not appear to be affected by the Limpopo Belt tectonics and metamorphism (Wilson and Prendergast 1988). They could possibly be related to late-stage crustal relaxation following the main orogenic event. The satellites cut across the study area into the Limpopo Belt; thus, their intrusion post-dates any major tectonic event within the belt (see below). In terms of tectono-magmatic events in the craton, the Plumtree dyke swarm of Wilson et al. (1987) also has the same trend but is restricted farther NW of the

study area where they have been associated with ~2150 Ma basaltic lavas of the Deweras Group (as their feeders?) in the Magondi Belt (Söderlund et al. 2010). Thus, the NNE fractures are associated with both the ~2.57 Ga Great Dyke and satellites, and the ~2150 Ma Plumtree swarm distinct ages implying two generations of 'dyking'.

At almost Great Dyke times, dykes of the 'Sebanga swarm' which is now dated between ~2.51 and ~2.41 Ga (Söderlund et al. 2010), with the Sebanga dyke (SPD, Figs. 2, 5, 6) at 2.41 Ga intruded into the NNW- to NW-trending extensional fractures. The NNW-trending extensional fractures also show multiple activity as dykes of the ca. 2000–1800 Ma Mashonaland Igneous Event (MIE) (Wilson et al. 1987; Wilson 1990), here represented by the widely spaced FRD dykes (D4, Fig. 11) (Figs. 6, 7, 11; Table 3), also intruded into these fractures. The FRD dykes have no detectable lateral displacement (Figs. 6 7 8), and therefore, strike-slip displacement was confined to the NW-trending Mchingwe and Jenya fault set. Minor dyke emplacement was contemporaneous with movements along these faults (e.g. Figs. 3, 6; Martin 1978). Based on similar palaeomagnetic directions, it has been assumed that the 'Sebanga dykes' (including the Crystal Springs mentioned earlier) are coeval with, and feeder dykes to, the ubiquitous ca. 1.9 Ga Mashonaland dolerites (Wilson et al. 1987). Wilson (1990) suggested that the MIE affected the entire craton and was sufficiently protracted to encompass major faulting and for some change in palaeomagnetic direction to be recorded in the intrusions, with negligible plate motion (Smirnov et al. 2013). This was partly based on earlier observations by Jones et al. (1975) in their study of dykes associated with the Great Dyke and later confirmed by Mushayandebvu et al. (1995) (see also Smirnov et al. 2013). These results are confirmed by observations on some of the NNW-trending dykes mapped in this study, such as the difference in magnetic signatures and horizontal displacements between the FRD dykes and the Sebanga dyke (Figs. 3, 4, 5, 6). Magnetic data show both positive and negative anomalies, suggesting the presence of dual-polarity (remanent) magnetisation. On the other hand, the Sebanga appears to have suffered more deformation as it is dismembered in several places while the others appear continuous. This would be in line with the new age of the SPD of 2408 Ma by Söderlund et al. (2010) using U–Pb on baddeleyite. Notably, all dykes associated with the MIE plus the older structures, including the Popoteke-Great Dyke set, cut through the NMZ but do not penetrate the Central Zone (CZ). This suggests that the ZC and NMZ were deformed together as an integral entity, separated from the CZ by shear zones (cf. Roering et al. 1992), and that the two were only juxtaposed after emplacement of the Great Dyke. Some workers document deformation and metamorphic event in the NMZ and CZ at 2.0 Ga, and postulate a link with the MIE (e.g. Jones et al. 1975, 1995; Wilson 1990; Mushayandebvu et al. 1994, 1995; Fedo et al. 1995; Kamber et al. 1995; Holzer et al. 1999; Blenkinsop 2011). Palaeomagnetic results from the southern part of the Sebanga dyke within the NMZ reveal a mean direction of magnetisation that is approximately reversed in declination, but with a substantially shallower inclination, compared to that obtained from the same dyke north of the NMZ (Mushayandebvu et al. 1995). However, results could not resolve whether this is a primary direction, or a younger overprint and/or a result of undetected tectonic tilting. Smirnov et al. (2013) propose the northern part to carry a primary remanence.

A subsequent widespread intraplate magmatic event at 1100 Ma formed the Umkondo Igneous Province (Wilson 1990), probably related to plume activity (e.g. Hanson et al. 1998, 2006), but these are mainly mafic dolerite sills that do not appear to be mapped in the study area. They are chemically different from the Mashonaland dolerites with higher SiO_2 and CaO contents (Stubbs 2000) and an entirely different palaeomagnetic direction (Wilson et al. 1987).

The youngest EW- to ESE–WNW-trending structures (D5, Fig. 11) have previously (Wilson et al. 1987; Ranganai 1995) been interpreted as part of the Botswana Karoo dyke swarm associated with lithospheric extension during the break-up of Gondwana (Duncan et al. 1997; Reeves 2000), but here we put forward an alternative interpretation. The obvious curvature in the interpreted dyke swarm in this study contrasts with the linear trend of the Botswana (Okavango) swarm, and it is possible that the identified (BKD) swarm is older as it appears to be cut across by the linear dykes. Further, an examination of the ZGS–BGS–CGS unpublished 1: 1 000 000 scale regional aeromagnetic maps (e.g. Fig. 12) suggests that the correlatives of the Botswana swarm occur south of the study area. It is noteworthy that these dykes, in turn, cut across the Great Dyke-related dykes (e.g. Umvimeela dyke; cf. Fig. 12), suggesting they could be Proterozoic in age (although no such trend has been observed on the 1.1 Ga Umkondo and 1.8 Ga Mashonaland Igneous intrusions). However, it is clear that both dyke swarms were intruded over periods spanning magnetic reversals, as they appear as alternating linear highs and lows (e.g. Figs. 2, 3, 4). It should also be noted that the timing and duration of this Karoo igneous event is currently a subject of debate (e.g. Duncan et al. 1997; Jones et al. 2001; Marsh 2002; Jourdan et al. 2004; Hanson et al. 2006). Jourdan et al. (2004) show that Proterozoic dykes and sills are also present in the Okavango (BKD) swarm (~10 % of all dykes), and relate these to the ~1.1 Ga Umkondo Igneous event (see also Marsh 2002). This is interpreted to imply that the dyke emplacement was controlled (or at least strongly influenced) by older

structures, and the geometry of the Karoo triple junction is not a pristine Jurassic structure (Jourdan et al. 2004, 2006). It is worth noting that the adjoining and coeval ENE-trending Sabi–Limpopo dyke swarm (D5) (Wilson et al. 1987; Jourdan et al. 2004, 2006; Le Gall et al. 2005; Hanson et al. 2006) is not seen in the area, and neither is it clearly mapped on the regional aeromagnetic map (Fig. 12). However, further east where the dykes are mapped south of the Masvingo greenstone belt (Gwavava and Ranganai 2009), they follow the Neoarchaean NMZ trend, again supporting basement control of dykes during the Karoo igneous events (Jourdan et al. 2006). This does not preclude the existence of lithospheric heterogeneities that may have guided melt generation, transport, and eruption sites.

Inferences on craton evolution

The integration of structural geology with the 3D analysis of potential field data provides a vital opportunity to link models of local architecture with models of the regional-scale architecture (Aitken and Betts 2009; Stewart et al. 2009). Parts of the study area have been used as examples of granite–gneiss and greenstone type areas for the rest of the craton (e.g. Bickle and Nisbet 1993; Wilson et al. 1995), and even the Archaean in general (e.g. Bickle and Nisbet 1993; Coward and Ries 1995; Dirks and Jelsma 2002; Hofmann and Kusky 2004). In a previous gravity study of the area, and based on similar geological structures, Ranganai et al. (2008) have extended their interpretation on greenstone belt geotectonic models to the whole craton with a caution that geophysical data alone cannot retrace the scheme of Archaean tectonics but offer tests of and constraints on geological and geochemical models. Significantly, an inspection of the various published and unpublished 1: 1 000 000 Zimbabwe aeromagnetic maps (e.g. Fig. 12) shows that some of the interpreted regional trends have representatives craton-wide (see also Wilson et al. 1987; Wilson 1990; Campbell et al. 1992). Typical examples are the NNE (Popoteke fault, PF), part of the Great Dyke fracture system, and the WNW trends (Gutu faults, GF) (Fig. 12; cf. Gwavava and Ranganai 2009) which may be part of the Mchingwe–Jenya fault set. We therefore suggest that the above discussions on the tectonic evolution of the study area generally apply to the rest of the craton. Cross-cutting structures and geochronological data (e.g. Taylor et al. 1991) show that the various dykes intruding the identified fractures and/or causing the lineament pattern were emplaced intermittently over a relatively long time. The parallelism of fault, shear, and dyke directions in the craton (Wilson et al. 1987; Wilson 1990; Campbell et al. 1992) suggests that the mafic magmas follow pre-existing zones of weakness. This implies that the orientation of these dykes is not only a result of the instantaneous stress field at the time of intrusion, but that the inherited fracture pattern played a decisive role (cf. Jourdan et al. 2006; Söderlund et al. 2010). Overall, it is clear that the craton experienced several episodes of heating, uplift and erosion and dyke emplacement (Wilson et al. 1987; Belton and Raab 2010; Blenkinsop 2011). Most of the lineaments are no doubt multiply reactivated features; geochronological data suggest that there may be more than one generation of dykes in a lineament (Jourdan et al. 2004; Söderlund et al. 2010).

Finally, we also note that the deeper crustal structure of the craton is poorly studied; thus, work is in progress to integrate the national aeromagnetic and gravity data sets to obtain a better picture, as has been done in several countries such as Australia, Canada, Namibia, and the USA (e.g. Gibson and Millegan 1998; Bauer et al. 2003). The integrated approach yields a higher confidence regional model (e.g. Aitken et al. 2008; Aitken and Betts 2009); the more information utilised, the more certain is the result of the inference (Nabighian et al. 2005). Further, recent palaeomagnetic work linking the ZC to the Yilgarn and other Archaean Cratons (e.g. Söderlund et al. 2010; Smirnov et al. 2013, and references therein) is of particular note in the scheme of worldwide plate tectonics.

Conclusions

Enhanced and processed aeromagnetic anomalies and their derivatives have allowed the mapped geology of the south-central Zimbabwe **C**raton to be extrapolated into areas of poor rock exposure, and revealed subsurface geometries of intrusive bodies, tectonic boundaries, and dyke swarms. Several previously unmapped faults, dykes, and ultramafic intrusions, only tentatively identified by geologic mapping alone, are now recognised. Shallow and deep depth slices of the magnetic field were able to separate the high-frequency anomalies from the low-frequency ones. The well-defined Euler solutions have confirmed the location of both pre-existing and the newly interpreted linear geological features, and gave estimates of their depths, thus confirming the geological significance of the qualitative interpretation. Structural and lithologic trends have therefore been established with much greater confidence than would be possible by magnetic anomaly–geology correlation alone. The intersection patterns of all these features provide relative age constraints on the time of crustal extension, dyke intrusion, and the Limpopo orogeny. A number of isolated deep Euler solutions are associated with ultramafic complexes, the Great Dyke, and the Umvimeela dyke, and these points could represent the original magma chambers and/or feeder points for these units.

In conclusion therefore, the aeromagnetic data and derived products, and the new map show that

1. The magnetic anomalies are closely associated with basement structures and bedrock lithology. In areas where geology is well mapped, these reflect rock petrology and metamorphic grade. Their interpretation, combined with gravity data, has led to a revised sub-outcrop map of the area (Fig. 11) showing improved structural detail. Spectral analysis results indicate a magnetic susceptibility discontinuity at 8.0 km depth, and this probably corresponds to a crustal boundary deduced from gravity and seismic data.
2. Five regional structural trends are identified (ENE, NNE, NNW, NW, and WNW) and correlated with various geological features and craton tectonic events, as well as more regional igneous events, resulting in a relative chronological order. These include a major NNW-trending dyke swarm associated with the widespread 1.8–2.0 Ga Mashonaland Igneous Event, and a continuation of the Botswana Karoo dyke swarm into southern parts of the Zimbabwe **C**raton and into the Limpopo Belt. The intrusion of the Karoo dykes, which is the youngest mafic event, is associated with fractures due to the break-up of Gondwana. The greenstone belts and related ultramafic complexes were an integral part of the lithosphere before much of the upper crustal (brittle?) deformation occurred.
3. The geostructural framework of the area is compatible with the postulated Late Archaean collision involving the Zimbabwe and Kaapvaal Cratons and the Limpopo Belt. The major inter- and intra-cratonic block movements associated with the Limpopo orogeny and other post-volcanic deformations (mainly due to granitic intrusions) produced structures or reactivated older fractures that were exploited by latest Archaean and Early Proterozoic mafic intrusions.
4. Using the various Euler solution maps and previous studies, the magnetic sources in the northern parts of the area (north of latitude 20.5°S or UTM 7740000N) are generally shallower by ~400 m than in the southern parts. This suggests that either the sources were emplaced at shallow levels or that the north probably experienced more uplift and higher erosion levels than the south. Alternatively, the southern parts could have been depressed by loading of the area by Limpopo Belt rocks thrust onto the southern edge of the craton.
5. Overall, structural evidence from the magnetic and gravity data, and the known geology suggest horizontal deformation as well as vertical crustal movements during the evolution of the area, with the former dominant from the Neoarchaean to the Proterozoic. There is a strong indication of coupling of forces in earlier stages. The interpreted regional trends have representatives craton-wide, implying that our inferences can be applied to the tectonic evolution of the craton as a whole with some confidence.

A final observation is that the structural interpretation results of this study emphasise the need as well as the relevance of examining the already available but unpublished 1: 1 000 000 scale regional gravity and aeromagnetic maps to study in detail the tectonic history of the Zimbabwe **C**raton as a whole, in conjunction with other geoscience techniques. The multidisciplinary investigations on crustal architecture will also clarify the link between continental basement geology, neotectonic, mineral and hydrocarbon exploration, hydrology, and geohazards.

Acknowledgments The Zimbabwe Geological Survey provided the aeromagnetic data used in this study and gave permission for the data to be published. This work represents part of postgraduate studies by RTR at the University of Leeds, funded by the Association of Commonwealth Universities, Commonwealth Scholarship Commission. RTR and KAW benefited from the British Council Link scheme between the Departments of Earth Sciences (University of Leeds) and Physics (University of Zimbabwe). RTR acknowledges initial contributions on this work from Dai Jones and Branko Corner, and thanks Alan Reid for advice and encouragement at various stages of the study. An extensive critical review by H Jelsma on the initial manuscript as well as comments by B Drenth and P Johnson on subsequent versions is greatly appreciated as they improved the paper. Constructive comments by the reviewers, especially Henry V Lyatsky, are greatly appreciated.

References

Airo M-L (2002) Aeromagnetic and aeroradiometric response to hydrothermal alteration. Surv Geophys 23:273–302

Aitken ARA, Betts PG (2009) Multi-scale integrated structural and aeromagnetic analysis to guide tectonic models: an example from the eastern Musgrave Province Central Australia. Tectonophysics 476(3–4):418–435

Aitken ARA, Betts PG, Schaefer BF, Rye SE (2008) Assessing uncertainty in the integration of aeromagnetic data and structural observations in the Deering Hills region of the Musgrave Province. Aust J Earth Sci 55(8):1127–1138

Allek K, Hamoudi M (2008) Regional-scale aeromagnetic survey of the south-west of Algeria: a tool for area selection for diamond exploration. J Afr Earth Sci 50:67–78

Barritt SD (1993) The African magnetic mapping project. ITC J 1993–2:122–131

Barton JM Jr, Holzer L, Kamber B, Doig R, Kramers JD, Nyfeler D (1994) Discrete metamorphic events in the Limpopo belt, southern Africa: implications for the application of P–T paths in complex metamorphic terrains. Geology 22:1035–1038

Bates MP, Mushayandebvu MF (1995) Magnetic fabric in the Umvimeela Dyke, satellite of the Great Dyke, Zimbabwe. Tectonophysics 242:241–254

Bauer K, Trumbull RB, Vietor T (2003) Geophysical images and a crustal model of intrusive structures beneath the Messum ring complex Namibia. Earth Planet Sci Lett 216(1/2):65–80

Becker JK, Siegesmund S, Jelsma H (2000) The Chinamora batholith, Zimbabwe: structure and emplacement-related magnetic rock fabric. J Struct Geol 22:1837–1853

Belton DX, Raab MJ (2010) Cretaceous reactivation and intensified erosion in the Archean-Proterozoic Limpopo Belt, demonstrated by apatite fission track thermochronology. Tectonophysics 480:99–108

Betts PG, Valenta R, Finlay J (2003) Evolution of the Mount Woods Inlier, northern Gawler Craton, Southern Australia: an integrated structural and aeromagnetic analysis. Tectonophysics 366:83–111

Betts PG, Williams H, Stewart J, Ailleres L (2007) Kinematic analysis of aeromagnetic data: looking at geophysical data in a structural context. Gondwana Res 11:582–583

Bickle MJ, Nisbet EG (eds) (1993) The geology of the Belingwe greenstone belt, Zimbabwe: a study of the evolution of Archaean continental crust. Geological Society of Zimbabwe Special Publication 2. A. A. Balkema, Rotterdam, p 239

Bickle MJ, Nisbet EG, Martin A (1994) Archean greenstone belts are not oceanic crust. J Geol 102:121–138

Blakely RJ (1995) Potential theory in gravity and magnetic applications. Cambridge University Press, Cambridge, p 441

Blenkinsop TG (2011) Archean magmatic granulites, diapirism, and Proterozoic reworking in the Northern Marginal Zone of the Limpopo Belt. Geol Soc Am Mem 207:1–24

Blenkinsop TG, Treloar PJ (1995) Geometry, classification and kinematics of SC and SC′ fabrics in the Mushandike area Zimbabwe. J Struct Geol 17(3):397–408

Blenkinsop TG, Mkweli S, Rollinson HR, Fedo CM, Paya BK, Kamber BS, Kramers JD, Berger M (1995) The North Limpopo Thrust Zone (NLTZ): the northern boundary of the Limpopo belt in Zimbabwe and Botswana. Ext Abstr Geol Soc S Afr Centen Geocongress 95:174–177

Blenkinsop TG, Martin A, Jelsma HA, Vinyu ML (1997) The Zimbabwe Craton. In: de Wit MJ, Ashwal LD (eds) Greenstone Belts. Oxford monograph on geology and geophysics, Oxford University Press, Oxford, pp 567–580

Blenkinsop TG, Kroner A, Chiwara V (2004) Single stage, late Archaean exhumation of granulites in the Northern Marginal Zone, Limpopo Belt, Zimbabwe, and relevance to gold mineralization at Renco Mine. S Afr J Geol 107:377–396

Bolhar R, Woodhead JD, Hergt JM (2003) Continental setting inferred for emplacement of the 2.9–2.7 Ga Belingwe Greenstone Belt, Zimbabwe. Geology 31: 295–298. (Comment and Reply; e30–e31)

Boshoff R, Van Reenen DD, Smit CA, Perchuk LL, Kramers JD, Armstrong R (2006) Geologic history of the Central Zone of the Limpopo Complex: the West Alldays Area. J Geol 114:699–716

Broome HJ (1990) Generation and interpretation of geophysical images with examples from the Rae Province, northwestern Canada Shield. Geophysics 55:977–997

Bumby AJ, Eriksson PG, Van Der Merwe R (2004) The early Proterozoic sedimentary record in the Blouberg area, Limpopo Province, South Africa: implications for the timing of the Limpopo orogenic event. J Afr Earth Sci 39:123–131

Campbell SDG, Pitfield PEJ (1994) Structural controls of gold mineralization in the Zimbabwe Craton- Exploration Guidelines. Zimbabwe Geological Survey Bulletin 101, Harare, pp 270

Campbell SDG, Oesterlen PM, Blenkinsop TG, Pitfield PEJ, Munyanyiwa H (1992) A Provisional 1:2 500 000 scale Tectonic map and the tectonic evolution of Zimbabwe. Ann Zimb Geol Surv XVI 1991:31–50

Carmichael RS (1982) Magnetic properties of minerals and rocks. In: Carmichael RS (ed) Handbook of Physical Properties of Rocks, vol 2. CRC Press, Boca Raton, pp 230–287

Carruthers RM, Greenbaum D, Jackson PD, Mtetwa S, Peart RJ, Shedlock SL (1993) Geological and geophysical characterisation of lineaments in southeast Zimbabwe and implications for groundwater exploration. Final Report, Technical Report WC/93/7, British Geological Survey, Keyworth, pp 234

Clark DA (1997) Magnetic petrophysics and magnetic petrology; aids to geological interpretation of magnetic surveys. J Aust Geol Geophys 17:83–103

Clark DA, Emerson DW (1991) Notes on rock magnetization characteristics in applied geophysical studies. Explor Geophys 22:547–555

Cooper GRJ, Cowan DR (2007) Enhancing linear features in image data using horizontal orthogonal gradient ratios. Comput Geosci 33:981–984

Coward MP, Ries AC (eds) (1995) Early precambrian processes, vol 95. Geological Society Special Publication, London, p 295

Coward MP, James PR, Wright L (1976) Northern margin of the Limpopo mobile belt, southern Africa. Geol Soc Am Bull 87:601–611

de Beer JH, Stettler EH (1992) The deep structure of the Limpopo Belt from geophysical studies. Precambr Res 55:173–186

De Wit MJ, Roering C, Hart RJ, Armstrong RA, De Ronde CEJ, Green RWE, Tredoux M, Peperdy E, Hart RA (1992) Formation of an archaean continent. Nature 357:553–562

Dirks PHGM, Jelsma HA (1998) Horizontal accretion and stabilization of the Archean Zimbabwe Craton. Geology 26(1):11–14

Dirks PHGM, Jelsma HA (2002) Crust-mantle decoupling and the growth of the Archaean Zimbabwe craton. J Afr Earth Sci 34:157–166

Dirks PHGM, Jelsma HA, Hofmann A (2002) Accretion of an Archaean greenstone belt in the Midlands of Zimbabwe. J Struct Geol 24:1707–1727

Dodson MH, Williams IS, Kramers JD (2001) The Mushandike granite: further evidence for 3.4 Ga magmatism in the Zimbabwe craton. Geol Mag 138:31–38

Duncan R, Hooper P, Rehacek J, March J, Duncan A (1997) The timing and duration of the Karoo igneous event, southern Gondwana. J Geophys Res 102:18127–18138

Durrheim RJ, Barker WH, Green RWE (1992) Seismic studies in the Limpopo belt. Precambr Res 55:187–200

Fedo CM, Errikson KA (1996) Stratigraphic framework of the ~3.0 Ga Buhwa Greenstone Belt: a unique stable-shelf succession in the Zimbabwe Archaean Craton. Precambr Res 77:161–178

Fedo CM, Eriksson K, Blenkinsop TG (1995) Geologic history of the Archean Buhwa Greenstone Belt and surrounding granite-gneiss terrane, Zimbabwe, with implications for the evolution of the Limpopo Belt. Can J Earth Sci 32:1977–1990

Ferraccioli F, Jones PC, Curtis ML, Leat PT, Riley TR (2005) Tectonic and magmatic patterns in the Jutulstraumen rift(?) region, East Antarctica, as imaged by high-resolution aeromagnetic data. Earth Planets Space 57:767–780

Frei R, Blenkinsop TG, Schönberg R (1999) Geochronology of the late Archaean Razi and Chilimanzi suites of granites in Zimbabwe: implications for the late Archaean tectonics of the Limpopo belt and Zimbabwe craton. S Afr J Geol 102:55–63

Geosoft (2004) Oasis Montaj (V5.1.8) and Euler 3D Deconvolution System (V5.1.5) manuals. Geosoft Inc., Toronto, Canada

Gibson RI, Millegan PS (eds) (1998) Geologic Applications of Gravity and Magnetics: Case Histories. Society of Exploration Geophysicists, Geophysical Reference Series 8, pp 162

Gore J, James DE, Zengeni TG, Gwavava O (2009) Crustal structure of the Zimbabwe craton and the Limpopo belt of Southern Africa: new constraints from seismic data and implications for its evolution. S Afr J Geol 112:213–228

Gwavava O, Ranganai RT (2009) The geology and structure of the Masvingo greenstone belt and adjacent granite plutons from geophysical data, Zimbabwe craton. S Afr J Geol 112:119–132

Gwavava O, Swain CJ, Podmore F, Fairhead DJ (1992) Evidence of crustal thinning beneath the Limpopo Belt and Lebombo monocline of southern Africa based upon regional gravity studies and implications for the reconstruction of Gondwana. Tectonophysics 212:1–20

Halls HC, Fahrig FW (eds) (1987) Mafic Dyke Swarms. Geological Association of Canada Special Paper 34. Toronto, Ontario, p 503

Hansen R, deRidder E (2006) Linear feature analysis for aeromagnetic data. Geophysics 71:L61–L67

Hanson RE, Martin MW, Bowring SA, Munyanyiwa H (1998) U-Pb zircon age for the Umkondo dolerites, eastern Zimbabwe: 1.1 Ga large igneous province in southern Africa–east Antarctica and possible Rodinia correlations. Geology 12:1143–1146

Hanson RE, Harmer RE, Blenkinsop TG, Bullen DS, Dalziel IWD, Gose WA, Hall RP, Kampunzu AB, Key RM, Mukwakwami J, Munyanyiwa H, Pancake JA, Seidel EK, Ward SE (2006) Mesoproterozoic intraplate magmatism in the Kalahari Craton: a review. J Afr Earth Sc 26:141–167

Hofmann A, Kusky T (2004) The Belingwe Greenstone Belt: ensialic or Oceanic? Dev Precambrian Geol 13:487–538

Hofmann A, Dirks PHGM, Jelsma HA, Matura N (2003) A tectonic origin for ironstone horizons in the Zimbabwe craton and their significance for greenstone belt geology. J Geol Soc Lon 160:83–97

Holzer L, Barton JM, Paya BK, Kramers JD (1999) Tectonothermal history of the western part of the Limpopo belt: tectonic models and new perspectives. J Afr Earth Sc 28:383–402

Horstwood MSA, Nesbitt RW, Noble SR, Wilson JF (1999) U-Pb zircon evidence for an extensive early Archean craton in Zimbabwe: a reassessment of the timing of craton formation, stabilization and growth. Geology 27:707–710

Hunter MA, Bickle MJ, Nisbet EG, Martin A, Chapman HJ (1998) Continental extensional setting for the Archean Belingwe greenstone belt, Zimbabwe. Geology 26:883–886

Jaques AL, Wellman P, Whitaker A, Wyborn D (1997) High-resolution geophysics in modern geological mapping. J Aust Geol Geophys 17(2):159–173

Jelsma HA, Dirks PHGM (2000) Tectonic evolution of a greenstone sequence in northern Zimbabwe: sequential early stacking and pluton diapirism. Tectonics 19:135–152

Jelsma HA, Dirks PHGM (2002) Neoarchaean tectonic evolution of the Zimbabwe Craton. In: Fowler CMR, Ebinger C, Hawkesworth CJ (eds) The Early Earth: Physical, Chemical and Biological Development. Geological Society of London, Special Publications 199, pp 183–211

Jelsma HA, van der Beek PA, Vinyu ML (1993) Tectonic evolution of the Bindura-Shamva greenstone belt (northern Zimbabwe): progressive deformation around diapiric batholiths. J Struct Geol 15:163–176

Jelsma HA, Vinyu ML, Valbracht PJ, Davies GR, Wijbrans JR, Verdurmen EAT (1996) Constraints on Archaean crustal evolution of the Zimbabwe craton: U-Pb zircon, Sm-Nd and Pb-Pb whole-rock isotope study. Contrib Mineral Petrol 124:55–70

Jelsma HA, Kröner A, Bozhko N, Stowe C (2004) Single zircon ages for two Archean banded migmatitic gneisses from central Zimbabwe. S Afr J Geol 107:577–586

Jones DL, Robertson IDM, McFadden PL (1975) A palaeomagnetic study of Precambrian dyke swarms associated with the Great Dyke of Rhodesia. Trans Geol Soc S Afr 77:339–413

Jones DL, Bates MP, Podmore F, Mushayandebvu MF (1995) The Great Dyke of Zimbabwe and its satellites: recent geophysical results and their implications. In: Srivastava RK, Chandra R (eds) Magmatism in Relation to Diverse Tectonic Settings. Oxford and IBH Publishing Co Pvt Ltd, Oxford, pp 209–222

Jones DL, Duncan RA, Briden JC, Randall DE, Mac-Niocaill C (2001) Age of the Batoka basalts, northern Zimbabwe, and the duration of Karoo large igneous province magmatism. Geochem Geophys Geosyst 2:1–15

Jourdan F, Feraud G, Bertrand H, Kampunzu AB, Tshoso G, Le Gall B, Tiercelin JJ, Capiez P (2004) The Karoo triple junction questioned: evidence from Jurassic and Proterozoic $^{40}Ar/^{39}Ar$ ages and geochemistry of the giant Okavango dyke swarm (Botswana). Earth Planet Sci Lett 222:989–1006

Jourdan F, Feraud G, Bertrand H, Watkeys MK, Kampunzu AB, Le Gall B (2006) Basement control on dyke distribution in Large Igneous Provinces: case study of the Karoo triple junction. Earth Planet Sci Lett 241:307–322

Kamber BS, Kramers JD, Napier R, Cliff RA, Rollinson HR (1995) The Triangle Shear zone, Zimbabwe, revisited: new data document an important event at 2.0 Ga. in the Limpopo Belt. Precambr Res 70:191–213

Kamber BS, Biino GG, Wijbrans JR, Davies GR, Villa IM (1996) Archaean granulites of the Limpopo belt, Zimbabwe: one slow exhumation or two rapid events? Tectonics 15(6):1414–1430

Kamber BS, Bolhar R, Webb GE (2004) Geochemistry of late Archaean stromatolites from Zimbabwe: evidence of microbial life in restricted epicontinental seas. Precambr Res 132:379–399

Kampunzu AB, Tombale AR, Zhai M, Bagai Z, Majaule T, Modisi MP (2003) Major and trace element geochemistry of plutonic rocks from Francistown, NE Botswana: evidence for a Neoarchaean continental active margin in the Zimbabwe craton. Lithos 71:431–460

Khoza D, Jones AG, Muller MR, Evans RL, Webb SJ, Miensopust M, The SAMTEX Team (2013) Tectonic model of the Limpopo Belt: constraints from magnetotelluric data. Precambr Res 226:143–156

Kreissig K, Holzer L, Frei R, Villa IM, Kramers JD, Kröner A, Smit CA, van Reenen DD (2001) Geochronology of the Hout River shear zone and the metamorphism in the Southern marginal zone of the Limpopo Belt, Southern Africa. Precambr Res 109:145–173

Kusky TM (1998) Tectonic setting and terrane accretion of the Archean Zimbabwe craton. Geology 26:163–166

Le Gall B, Tshoso G, Dyment J, Kampunzu AB, Jourdan F, Fe´raud G, Bertrand H, Aubourg C, Ve´tel W (2005) The Okavango giant mafic dyke swarm (NE Botswana): its structural significance within the Karoo Large Igneous Province. J Struct Geol 27:2234–2255

Lee MK, Pharaoh TC, Soper NJ (1990) Structural trends in central Britain from images of gravity and aeromagnetic fields. J Geol Soc Lon 147:241–258

Marsh JS (2002) Discussion on 'The geophysical mapping of Mesozoic dyke swarms in southern Africa and their origin in the disruption of Gondwana'. J Afr Earth Sc 35:525–527

Martin A (1978) The geology of the Belingwe-Shabani schist belt. Rhod Geol Surv Bull 83:220

McDonald AJW, Fletcher CJN, Carruthers RM, Wilson D, Evans RB (1992) Interpretation of the regional gravity and magnetic surveys of Wales, using shaded relief and Euler deconvolution techniques. Geol Mag 129:523–531

Mekonnen TK (2004) Interpretation & Geodatabase of dykes using aeromagnetic data of Zimbabwe and Mozambique. MSc Thesis, ITC, Enschede, Netherlands. p 72

Mkweli S, Dirks PHGM (1997) What happens at the margin of the Zimbabwe Craton and the Limpopo belt?. Geological Society of Zimbabwe, Abstract Volume, Intraplate Magmatism and Tectonics of southern Africa p 35

Mkweli S, Kamber B, Berger M (1995) Westward continuation of the craton-Limpopo Belt tectonic break in Zimbabwe and new age constraints on the timing of the thrusting. J Geol Soc Lon 152:77–83

Moody JB (1976) Serpentinisation: a review. Lithos 9:125–138

Mukasa SB, Wilson AH, Carlson RW (1998) A multielement geochronologic study of the Great Dyke, Zimbabwe: significance of the robust and reset ages. Earth Planet Sci Lett 164(1/2):353–369

Mushayandebvu MF (1995) Magnetic modelling of the Umvimeela and East dykes: evidence for regional tilting of the Zimbabwe craton adjacent to the Limpopo Belt. J Appl Sci South Afr 1:47–58

Mushayandebvu MF, Jones DL, Briden JC (1994) A palaeomagnetic study of the Umvimeela Dyke, Zimbabwe: evidence for a Mesoproterozoic overprint. Precambr Res 69:269–280

Mushayandebvu MF, Jones DL, Briden JC (1995) Palaeomagnetic and geochronological results from Proterozoic mafic intrusions in southern Zimbabwe. In: Baer G, Heimann A (eds) Physics and Chemistry of Dykes. A.A. Balkema, Rotterdam, pp 293–303

Nabighian MN, Grauch VJ, Hansen RO, LaFehr TR, Li Y, Peirce JW, Phillips JD, Ruder ME (2005) The historical development of the magnetic method in exploration. Geophysics 70:33–61

Nguuri TK, Gore J, James DE, Wright C, Zengeni TG, Gwavava O, Webb SJ, Snoke JA (2001) Crustal structure beneath southern Africa and its implications for the formation and evolution of the Kaapvaal and Zimbabwe cratons. Geophys Res Lett 28:2501–2504

Oberthür T, Davis DW, Blenkinsop TG, Höhndorf A (2002) Precise U-Pb mineral ages, Rb-Sr and Sm-Nd systematics of the Great Dyke, Zimbabwe: constraints on late Archean events in the Zimbabwe Craton and Limpopo Belt. Precambr Res 113:293–305

Parker AJ, Rickwood PC, Tucker DH (eds) (1990) Mafic Dykes and emplacement mechanisms. Proceedings of 2nd international dyke conference, Adelaide, Australia. A.A. Balkema, Rotterdam, pp 641

Percival JA, West GF (1994) The Kapuskasing uplift: a geological and geophysical synthesis. Can J Earth Sci 31:1256–1286

Pilkington M, Keating P (2004) Contact mapping from gridded magnetic data—a comparison of techniques. Explor Geophys 35:306–311

Prendergast MD (2004) The Bulawayan Supergroup: a late Archaean passive margin-related large igneous province in the Zimbabwe craton. J Geol Soc 161(3):431–445

Prendergast MD, Wingate MTD (2007) Zircon geochronology and partial structural re-interpretation of the late Archaean Mashaba Igneous Complex, south-central Zimbabwe. S Afr J Geol 110(4):585–596

Ranganai RT (1995) Geophysical Investigations of the Granite-Greenstone Terrain in the South-Central Zimbabwe Archaean Craton. PhD Thesis, University of Leeds, Leeds, pp 288

Ranganai RT (2012) Euler deconvolution and spectral analysis of regional aeromagnetic data from the south-central Zimbabwe Craton: tectonic implications. Afr J Sci Technol (AJST) Science and Engineering Series 12(1):34–50

Ranganai RT (2013) Structural and subsurface relationships between the Fort Rixon-Shangani Greenstone Belt and the Nalatale Pluton, Zimbabwe, as derived from gravity and aeromagnetic data. S Afr J Geol 116(2):273–296

Ranganai RT, Ebinger CJ (2008) Aeromagnetic and LANDSAT TM structural interpretation for identifying regional groundwater exploration targets, south-central Zimbabwe Craton. J Appl Geophys 65:73–83

Ranganai RT, Mhindu C (2003) Aeromagnetic and landsat TM structural interpretation and GIS-based definition of mineral exploration targets, South-Central Zimbabwe Craton. 8th SAGA biennial technical meeting and exhibition, 7-10 October 2003, Pilanesberg, RSA, Extended Abstracts CD-Rom, pp 4

Ranganai RT, Kampunzu AB, Atekwana EA, Paya BK, King JG, Koosimile DI, Stettler EH (2002) Gravity Evidence for a larger Limpopo Belt in Southern Africa and geodynamic implications. Geophys J Int 149:9–14

Ranganai RT, Whaler KA, Ebinger CJ (2008) Gravity anomaly patterns in the south-central Zimbabwe (Archaean) craton and their geological interpretation. J Afr Earth Sc 51(5):257–276

Reeves CV (1989) Aeromagnetic interpretation and rock magnetism. First Break 7:275–286

Reeves CV (2000) The geophysical mapping of Mesozoic dyke swarms in southern Africa and their origin in the disruption of Gondwana. J Afr Earth Sc 30:499–513

Reeves CV, Reford SW, Milligan PR (1997) Airborne geophysics-old methods, new images. In: Gubbins AG (ed) Proceedings of Exploration'97: Fourth Decennial International Conference on Mineral Exploration, pp 13–30

Reid AB, Allsop JM, Granser H, Millet AJ, Somerton IW (1990) Magnetic interpretation in three dimensions using Euler deconvolution. Geophysics 55:80–91

Robertson IDM (1973) Potash granites of the southern edge of the Rhodesian craton and the northern granulite zone of the Limpopo belt. Geol Soc S Afr Spec Publ 3:265–276

Roering C, van Reenen DD, Smit C, Barton JM Jr, de Beer JH, de Wit MJ, Stettler EH, van Schalkwyk JF, Stevens G, Pretorious S (1992) Tectonic model for the evolution of the Limpopo belt. Precambr Res 55:539–552

Rollinson HR (1993) A terrane interpretation of the Archaean Limpopo Belt. Geol Mag 130:755–765

Rollinson HR, Blenkinsop TG (1995) The magmatic, metamorphic and tectonic evolution of the Northern Marginal Zone of the Limpopo Belt in Zimbabwe. J Geol Soc London 152:65–75

Schaller M, Steiner O, Studer I, Holzer L, Herwegh M, Kramers JD (1999) Exhumation of Limpopo Central Zone granulites and dextral continent-scale transcurrent movement at 2.0 Ga along the Palala Shear Zone, Northern Province South Africa. Precambrian Res 96:263–288

Schoenberg R, Nägler TF, Gnos E, Kramers JD, Kamber BS (2003) The source of the Great Dyke, Zimbabwe, and its tectonic significance: evidence from Re-Os isotopes. J Geol 111:565–578

Schwarz EJ, Hood PJ, Teskey DJ (1987) Magnetic expressions of Canadian diabase dykes and downward modeling. In: Halls HC, Fahrig WF (eds) Mafic dyke swarms, Geological Association of Canada Special Paper 34:153–162

Siegesmund S, Jelsma H, Becker J, Davies G, Layer P, van Dijk E, Kater L, Vinyu M (2002) Constraints on the timing of granite emplacement, deformation and metamorphism in the Shamva area, Zimbabwe. Int J Earth Sci 91:20–34

Smirnov AV, Evans DAD, Ernst RE, Söderlund U, Li Z-X (2013) Trading partners: tectonic ancestry of southern Africa and western Australia, in Archean supercratons Vaalbara and Zimgarn. Precambr Res 224:11–22

Smith WHF, Wessel P (1990) Gridding with continuous curvature splines in tension. Geophysics 55:293–305

Söderlund U, Hofmann A, Klausen MB, Olsson JR, Ernst RE, Persson P (2010) Towards a complete magmatic barcode for the Zimbabwe craton: baddeleyite U-Pb dating of regional dolerite dyke swarms and sill complexes. Precambr Res 183:388–398

Spector A, Grant FS (1970) Statistical models for interpreting aeromagnetic data. Geophysics 35:293–302

Stettler EH, de Beer JH, Blom MP (1989) Crustal domains in the northern Kaapvaal craton as defined by magnetic lineaments. Precambr Res 45:263–276

Stewart JR, Betts PG, Collins AS, Schaefer BF (2009) Multi-scale analysis of Proterozoic shear zones: an integrated structural and geophysical study. J Struct Geol 31:1238–1254

Stowe CW (1980) Wrench tectonics in the Archaean Rhodesian craton. Trans Geol Soc S Afr 83:193–205

Stubbs HM (2000) The geochemistry and petrogenesis of the Archaean and Palaeoproterozoic dykes and sills of Zimbabwe. PhD thesis, University of Portsmouth, UK

Stubbs HM, Hall PR, Hughes DJ, Nesbitt RW (1999) Evidence for a high Mg andesitic parental magma to the East and West satellite dykes of the Great Dyke, Zimbabwe: comparison with the continental tholeiitic Mashonaland sills. J Afr Earth Sci 28(2):325–336

Talwani P, Wildermuth E, Parkinson CD (2003) An impact crater in northeast South Carolina inferred from potential field data. Geophys Res Lett 30(7):1366. doi:10.1029/2003GL017051

Taylor PN, Kramers DJ, Moorbath S, Wilson JF, Orpen JL, Martin A (1991) Pb/Pb, Sm-Nd and Rb-Sr geochronology in the Archaean craton of Zimbabwe. Chem Geol (Isotope Geosci) 87:175–196

Teskey DJ, Hood PJ (1991) The Canadian aeromagnetic database: evolution and applications to the definition of major crustal boundaries. Tectonophysics 192:41–56

Treloar PJ, Blenkinsop TG (1995) Archaean deformation patterns in Zimbabwe: true indicators of Tibetan-style crustal extrusion or not? In: Coward MP, Ries AC (eds) Early Precambrian Processes, Geological Society Special Publication 95: 87–108

Treloar PJ, Coward MP, Harris NBW (1992) Himalayan-Tibetan analogies for the evolution of the Zimbabwe Craton and Limpopo Belt. Precambr Res 55:571–587

Uken R, Watkeys MK (1997) An interpretation of mafic dyke swarms and their relationship with major mafic and magmatic events on the Kaapvaal Craton and Limpopo belt. S Afr J Geol 100(4):341–348

Verduzco BJ, Fairhead D, Green CM, MacKenzie C (2004) New insights into magnetic derivatives for structural mapping. Lead Edge 23:116–119

Wilson JF (1990) A craton and its cracks: some of the behaviour of the Zimbabwe block from the Late Archaean to the Mesozoic in response to horizontal movements, and the significance of some of its mafic dyke fracture patterns. J Afr Earth Sc 10:483–501

Wilson AH, Prendergast DM (1988) The Great Dyke of Zimbabwe-I: tectonic setting, stratigraphy, petrology, structure, emplacement and crystallization. In: Prendergast MD, Jones MJ (eds) Magmatic Sulphides- the Zimbabwe Volume. IMM, London, pp 1–20

Wilson JF, Jones DL, Kramers JD (1987) Mafic dyke swarms in Zimbabwe. In: Halls HC, Fahrig WF (eds) Mafic Dyke Swarms, Geological Association of Canada Special Paper 34: 433–444

Wilson JF, Nesbitt RW, Fanning CM (1995) Zircon geochronology of Archaean felsic sequences in the Zimbabwe **C**raton: a revision of greenstone stratigraphy and a model for crustal growth. In: Coward MP, Ries AC (eds) Early precambrian processes, Geological Society Special Publication 95:109–126

Wolfenden E, Ebinger C, Yirgu G, Deino A, Ayalew D (2004) Evolution of the northern Main Ethiopian rift: birth of a triple junction. Earth Planet Sci Lett 224:213–228